2-P

DISCRETE CONTROL OF LINEAR DISTRIBUTED SYSTEMS WITH APPLICATION TO THE DEFORMABLE PRIMARY MIRROR OF A LARGE ORBITING TELESCOPE

BY

JEREMIAH F. CREEDON

A THESIS SUBMITTED IN PARTIAL FULFILLMENT OF THE REQUIREMENTS FOR THE DEGREE OF

DOCTOR OF PHILOSOPHY

IN

ELECTRICAL ENGINEERING

UNIVERSITY OF RHODE ISLAND

1970

DISCRETE CONTROL OF LINEAR DISTRIBUTED SYSTEMS WITH APPLICATION TO THE DEFORMABLE PRIMARY MIRROR OF A LARGE ORBITING TELESCOPE

ABSTRACT

One of the more significant technological problems associated with the orbital operation of large astronomical telescopes is the fabrication and maintenance of the primary mirror surface to the tolerance required for diffraction-limited performance. An interesting approach to the solution of this problem involves continuously measuring and automatically correcting the optical surface of a thin deformable mirror by means of discrete actuators located on its rear surface. The realization of diffraction-limited performance from a telescope in space by this method rests on the ability of the designer to achieve extremely accurate control of a highly complex, interacting, multivariable system. This paper presents the results of a detailed study of the discrete control of linear distributed systems with specific application to the design of a practical controller for a plant representative of a telescope primary mirror for an orbiting astronomical observatory.

The problem of controlling the distributed plant is treated by employing modal techniques to represent variations in the optical figure. Distortion of the mirror surface, which arises primarily from thermal gradients, is countered by actuators working against a backing structure to apply a corrective force distribution to the controlled surface. Each displacement actuator is in series with a spring attached

to the mirror by means of a pad intentionally introduced to restrict the excitation of high-order modes. Control is then exerted over a finite number (equal to the number of actuators) of the most significant modes.

Through the application of the modal expansion technique the mirror equation of motion is transformed to a set of uncoupled, linear, time-invariant, ordinary differential equations. The desired dynamic response and static accuracy may then be achieved by the application of classical single-variable design techniques. The formulation of a quadratic performance index which incorporates a measure of image quality permits determination of the trade-off between the number of actuators and optical purity. A criterion for defining actuator placement and pad size is presented which minimizes the tendency of the controller to excite the unmonitored modes.

DOCTOR OF PHILOSOPHY THESIS

OF

JEREMIAH F. CREEDON

Approved:

Thesis Committee:

Chairman _____

_____

_____

_____

Dean of the Graduate School

UNIVERSITY OF RHODE ISLAND

1970

ACKNOWLEDGMENTS

The author wishes to acknowledge the administrative officers of the NASA Langley Research Center, the Flight Instrumentation Division, and the Navigation and Guidance Research Branch for their cooperation in permitting the author to pursue the research which led to this thesis.

The author is particularly indebted to his major advisor, Prof. A. G. Lindgren for his encouragement, guidance, and technical suggestions.

The patience and encouragement of the author's wife, Gail, and children have been factors of primary importance in enabling him to complete this work.

TABLE OF CONTENTS

LIST OF FIGURES

I. INTRODUCTION

The class of distributed plants considered in this paper is restricted to those described by linear, time-invariant, separable operators where control is derived from a finite number of discrete inputs. Application of the modal expansion approach[1] converts the distributed-parameter problem to one of a multivariable nature which readily yields to decoupling techniques.[2] Classical single-variable control methods are applied to decoupled system dynamics defined in terms of the eigenvalues of the linear operator whose eigenfunctions are assumed to form a complete orthonormal set. While the results are applicable to the general problem of controlling linear distributed systems, the motivation for the study is a direct result of its relevance to one of the central problems of large orbiting telescope technology.

Elimination of the effects of the earth's atmosphere give orbiting telescopes significant advantages relative to earth-based telescopes. Figure 1 displays percent transmission of the incident radiation through the earth's atmosphere as a function of wavelength.[3] In the portion of the spectrum shown, the earth's atmosphere is opaque to radiation shorter than 3×10^{-5} cm and longer than 3×10^{-3} cm, with numerous gaps between these extremes. Since the entire spectrum of radiated energy becomes available for study in an atmosphere-free environment the additional spectral coverage would permit studies involving galactic nebulae and cool stars (stellar evolution).[4]

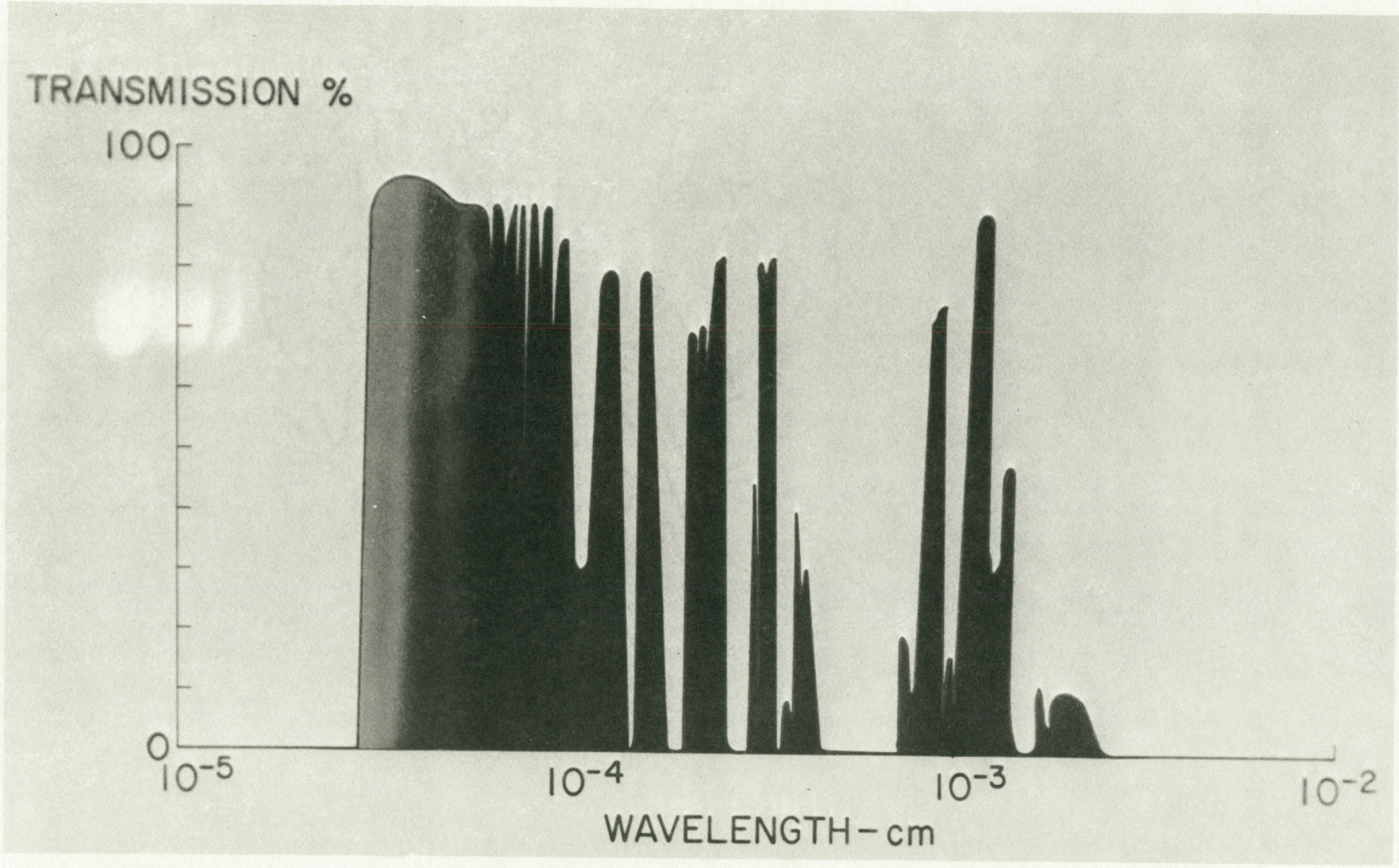

Figure 1.- Transmission of incident radiation through the earth's atmosphere.

Secondly, refraction anomalies associated with the turbulence of the earth's atmosphere limit the resolving power of earth-based telescopes; consequently, the 200-inch (508 cm) Hale telescope at Mt. Palomar has no better resolution than a high quality telescope of approximately 15 inches (38 cm) diameter.(5) Placing a 120-inch (3 meter) telescope in orbit would yield an increase in resolution of at least a factor of 7 relative to land-based telescopes and 3 relative to present space telescopes. This significant improvement is useful in studying double stars and in planetary photography.(4) Figure 2 shows two views of the same portion of the lunar surface. The photograph on the right was taken by the 120-inch (3 meter) reflector at the Lick Observatory and represents about the best resolution available from an earth-based telescope. On the left is a Lunar Orbiter photograph of the same area which has been selected to show the resolution available from the same size telescope outside of the atmosphere. Further, elimination of the background glow associated with the atmosphere would permit longer exposure times in celestial photography, effectively enabling astronomers to see deeper into space. Realization of these advantages is contingent upon solving several technological problems.

One of the more significant of these problems and the one which motivated the present investigation is the fabrication and maintenance of the primary mirror surface to the tolerance required for diffraction-limited performance. For the purpose of this paper, diffraction-limited performance is defined as being obtained when the rms figure error over the mirror surface is less than a fiftieth of a wavelength, which

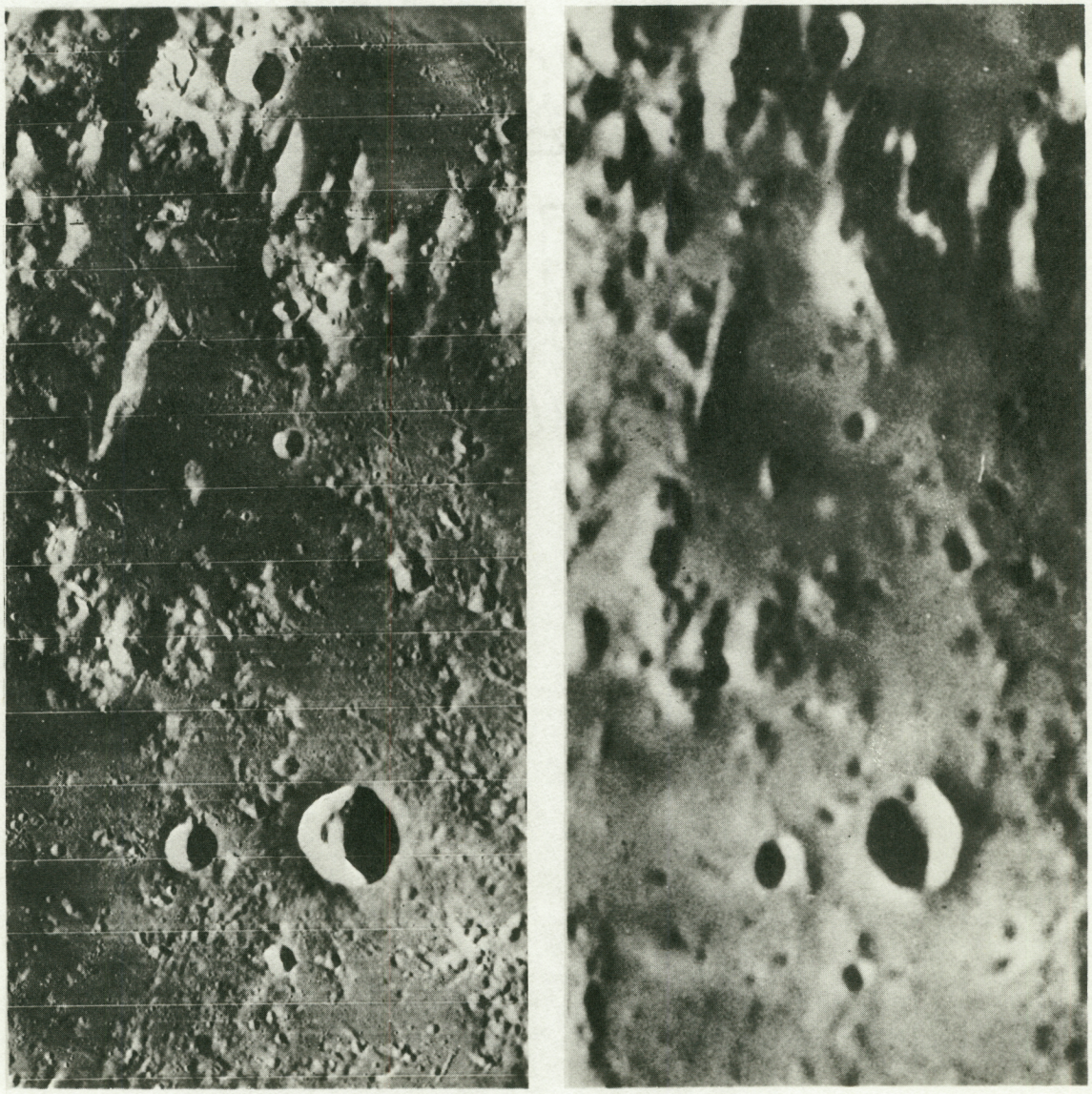

Figure 2.- Two views of the lunar surface indicating the increased resolution available from an orbiting telescope.

at 6328 Å is 1/2-μ inch (1.27×10^{-6} cm). It is extremely difficult to achieve this accuracy with the monolithic mirror normally used in telescope applications as uncorrected thermal gradients, fabrication in a one "g" and operation in a zero "g" environment, and material reaction to stresses introduced during figuring all tend to cause distortion of the mirror surface.

An interesting approach which has been investigated as a means of solving the problem involves measuring the deviation of the mirror figure from the desired shape, generating the necessary control signals, and applying these signals to physically align the mirror to the desired shape. This concept, which is shown schematically in Fig. 3, has been investigated with both a segmented and a thin deformable mirror. The segmented mirror consists of a number of individual pieces or segments. This approach was selected because many of the effects causing surface deformations are reduced on mirrors of small size. In a Cassegrain telescope the incoming light is reflected by the primary and secondary mirror to focus behind the primary. In this case, the primary is also illuminated by monochromatic light which is returned to the mirror figure error sensor. The error signal is then processed and applied to the actuators which correct each segment in tilt and focus.

This concept has been successfully applied to a small segmented mirror.[6, 7]. However, the construction of large segmented primary mirrors from individually fabricated off-axis portions of a paraboloid (matched in focal length) would require new techniques of fabricating

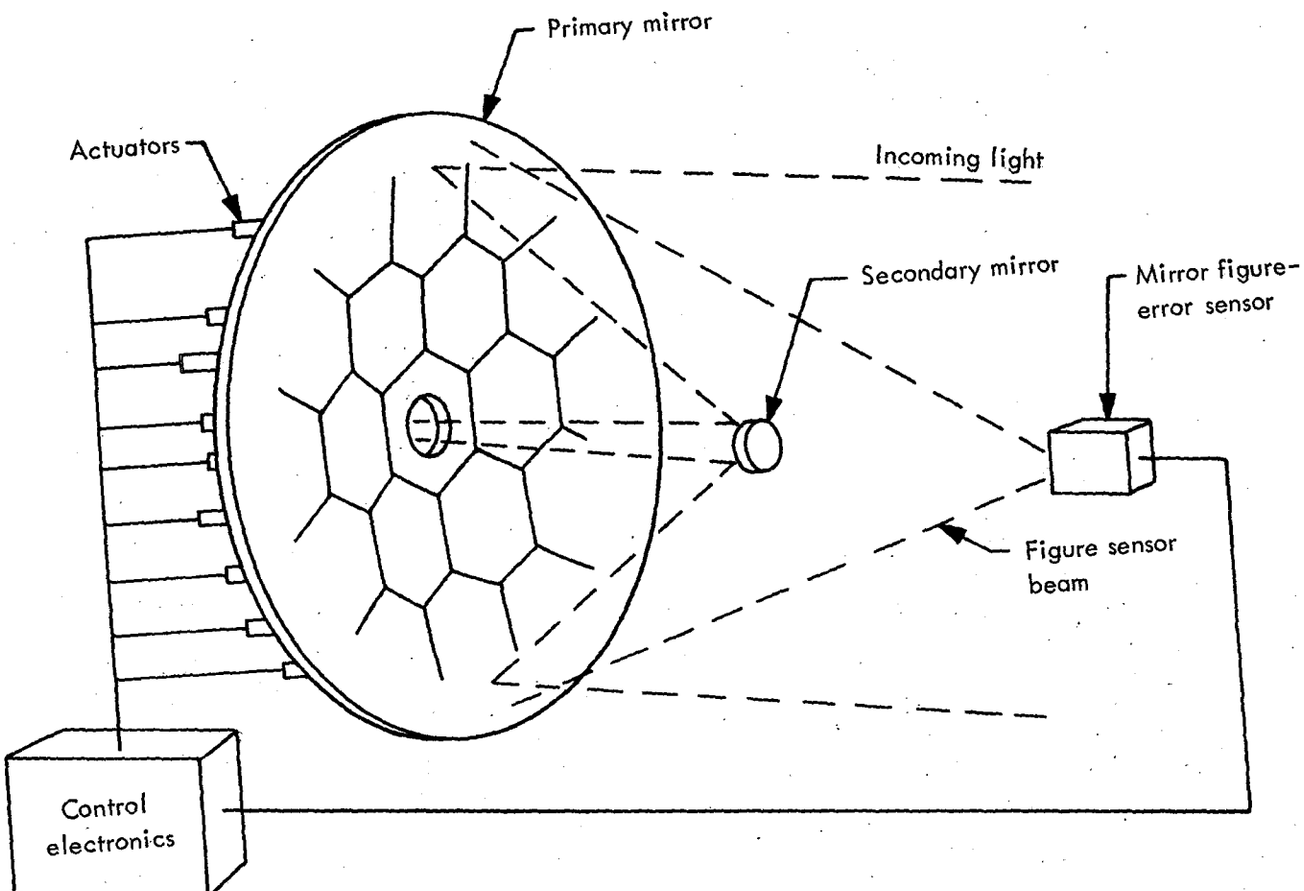

Figure 3.- Schematic representation of a system for controlling the optical surface of a telescope primary mirror.

diffraction-limited aspherics. In addition, the segmented mirror consists of a number of monolithic mirrors each subject to the same limitations as a monolithic mirror. While these limitations are reduced in the relatively small segments, they are still of sufficient magnitude to require that the segments be fabricated from a substance which exhibits a very high degree of material stability. This is because the segments are corrected in tilt and focus only and any warping of a segment cannot be completely corrected.

An alternate approach involves a thin, continuous-surface, deformable mirror that can be stressed into the desired shape by means of a large number of actuators arrayed across its rear surface. The greater control flexibility inherent in this approach shows promise of relaxing the material stability and fabrication tolerance requirements. A laboratory model of a thin mirror is shown in Fig. 4 alongside a conventional monolithic mirror. The thin mirror is 30 inches (76.2 cm) in diameter and 0.5 inches (1.27 cm) thick. Actuators were located every 3-3/4 inches (9.46 cm) over the rear surface of the mirror and were used to apply a corrective force distribution.[8] Preliminary operation of the system indicates that the actuators were able to reduce the initial figuring error to acceptable levels. This is illustrated in Fig. 5 which displays photographs of the diffraction pattern of the mirror before and during control.

While this application appears to demonstrate the ability of the thin mirror approach to enhance the telescope performance, a number of areas exist in which an improved design technique would be of significant

Figure 4.- Comparison of a thin deformable mirror with a mirror of normal thickness-to-diameter ratio.

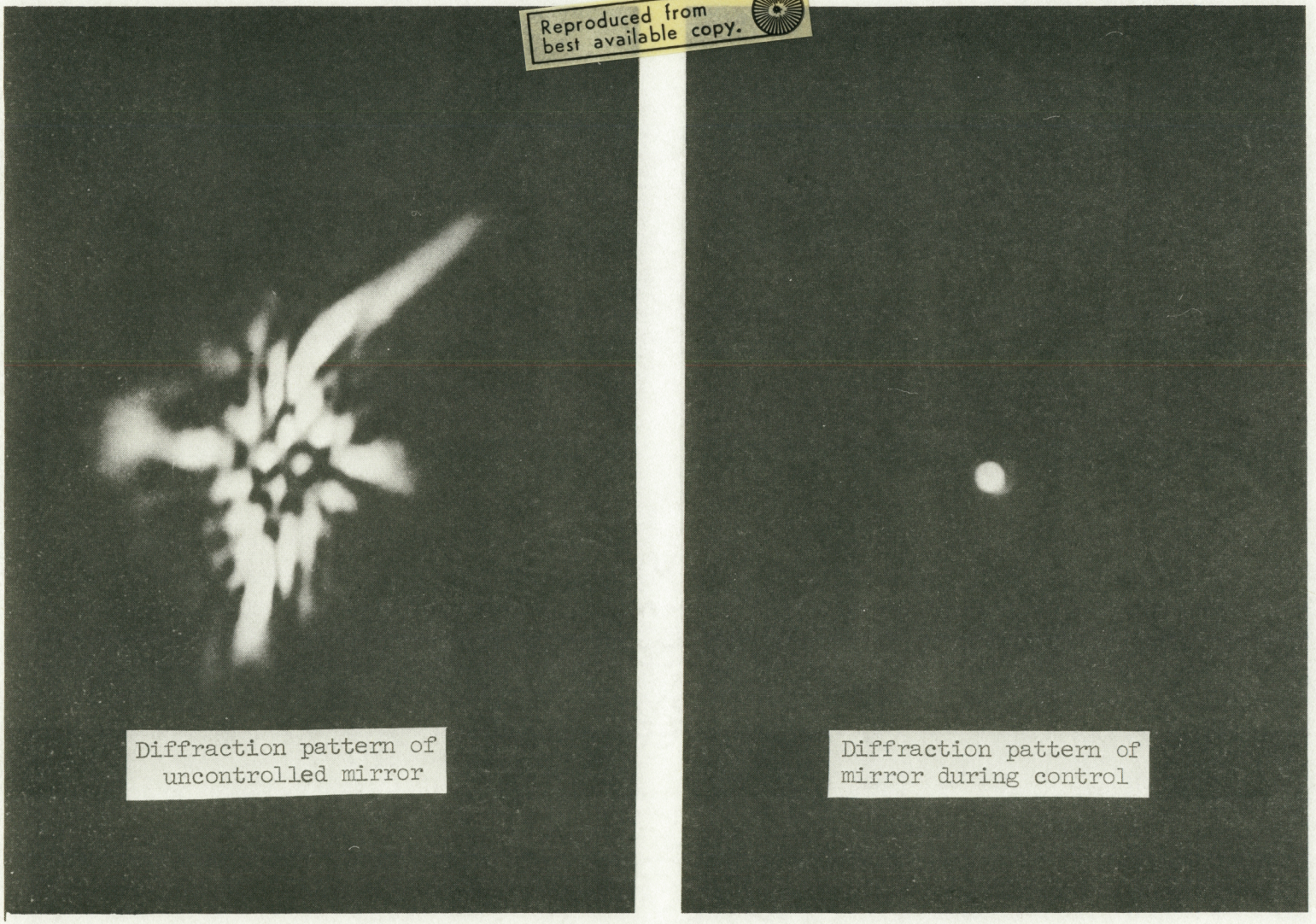

Figure 5.- Comparison of the diffraction pattern of the uncontrolled mirror with that of the mirror during control.

value. In present design efforts the dynamics of the plant have been largely ignored. This is a significant factor in the control of larger mirrors which have very lightly damped low frequency resonances. Selection and placement of the actuators is presently done on an arbitrary basis as a result of the present limited ability to relate the effects of these design decisions to system performance. In addition, the ability to more completely incorporate information on the disturbance characteristics, to the extent that it becomes available, is desirable.

The purpose of this paper is to present a general theory for the discrete control of a distributed-parameter system and extend the modal expansion technique to completely specify system performance. In the past little research effort has been devoted to the problem of obtaining discrete control of distributed-parameter systems and the results which have been obtained by Gould and Murry-Lasso[1] are limited to plants which have finite modal content. In this thesis the entire modal structure of the plant is considered for the problem of obtaining a specified level of performance while minimizing the number of control inputs to the plant. The method is demonstrated with examples and results are presented for a plant representative of a thin deformable mirror.

II. MODAL EXPANSION TECHNIQUE

A schematic representation of the plant under consideration is shown in Fig. 6 where L is a linear, time-invariant, separable operator. A typical example of a distributed system is the thin rectangular plate of Fig. 7, where the deflection normal to the midplane of the plate $w(x,y,t)$ results from the application of a transverse load density $p(x,y,t)$. The equation of motion of the plate is given by[9]

$$\nabla^2 S \nabla^2 w(x,y,t) + \rho \frac{\partial^2}{\partial t^2} w(x,y,t) = p(x,y,t) \qquad [1]$$

where ∇^2 is the Laplacian in Cartesian coordinates, ρ the mass per unit area, and $S = Yh^3/12(1 - \nu^2)$ is the flexural stiffness modulus of the plate. The deflection, $w(x,y,t)$, is assumed separable, i.e.,

$$w(x,y,t) = c_i(t)u_i(x,y). \qquad [2]$$

Substituting [2] into the homogeneous form of [1] yields, for a homogeneous plate of uniform thickness,

$$\frac{d^2c_i(t)}{dt^2} + \omega_i^2 c_i(t) = 0 \qquad [3a]$$

and

$$\frac{S}{\rho} \nabla^4 u_i(x,y) - \omega_i^2 u_i(x,y) = 0 \qquad [3b]$$

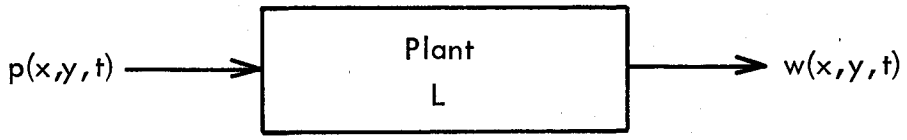

Figure 6.- Operator representation of the plant.

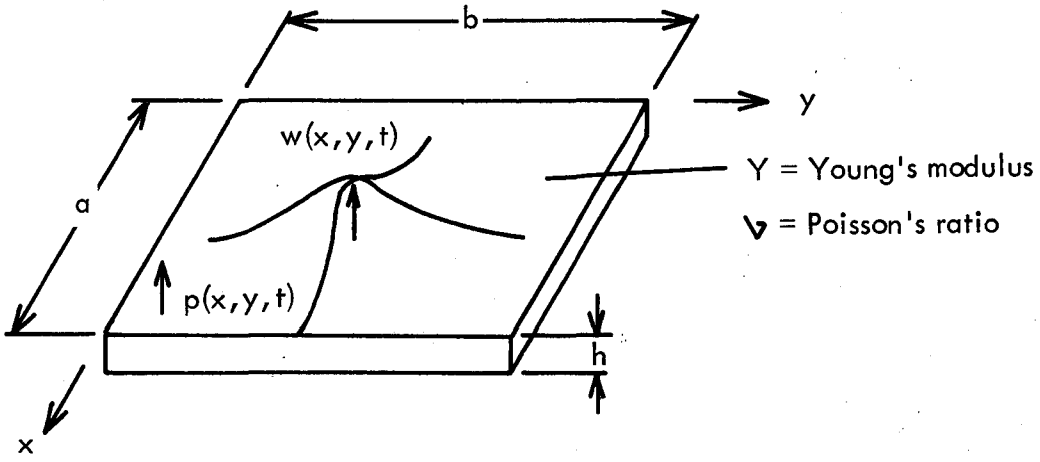

Figure 7.- Flat rectangular plate.

where ω_i^2 is a constant whose value is specified by the boundary conditions. For the simply supported plate, which has boundary conditions[10]

$$u_i(0,y) = u_i(a,y) = u_i(x,0) = u_i(x,b) = 0, \qquad [4a]$$

$$\frac{\partial^2}{\partial x^2} u_i + \nu \frac{\partial^2}{\partial y^2} u_i \Bigg|_{x = 0,a} = 0, \qquad [4b]$$

and

$$\nu \frac{\partial^2}{\partial x^2} u_i + \frac{\partial^2}{\partial y^2} u_i \Bigg|_{y = 0,b} = 0, \qquad [4c]$$

there exists[11] a denumerably infinite sequence

$$\omega_i = \omega_{mn} = \sqrt{\frac{S}{\rho}} \left[\left(\frac{m\pi}{a} \right)^2 + \left(\frac{n\pi}{b} \right)^2 \right] \qquad [5a]$$

where m, n = 1, 2, ... are the mode indices corresponding to the eigenfunctions

$$u_i = u_{mn}(x,y) = \frac{4}{ab} (\sin m \frac{\pi}{a} x)(\sin n \frac{\pi}{b} y) \qquad [5b]$$

which form a complete orthonormal set (Appendix A). Consequently, the general solution to Eq. [1] is

$$w(x,y,t) = \sum_{i=1}^{\infty} c_i(t)u_i(x,y) = \sum_{m,n=1}^{\infty} c_{mn}(t)u_{mn}(x,y) \qquad [6a]$$

and since the u_i form a complete set the loading may be expanded in a uniformly convergent series of the form

$$p(x,y,t) = \sum_{i=1}^{\infty} a_i(t)u_i(x,y) = \sum_{m,n=1}^{\infty} a_{mn}(t)u_{mn}(x,y) \qquad [6b]$$

where

$$a_i(t) = \iint_{\Gamma} p(x,y,t)u_i(x,y)dx\ dy \qquad [6c]$$

and Γ is the spatial region in which the plant is defined.

Substituting [6a], [6b], and [3b] into [1] and taking the Laplace transform with respect to time yields

$$\sum_{i=1}^{\infty} (s^2 + \omega_i^2)c_i(s)u_i(x,y) = \frac{1}{\rho}\sum_{i=1} a_i(s)u_i(x,Y) \qquad [7]$$

where s is the Laplacian operator and, for convenience, the same symbol is used to denote a variable and its Laplace transform. Since the $u_i(x,y)$ are independent the coefficients may be equated yielding

$$c_i(s) = \lambda_i(s)a_i(s) \qquad [8a]$$

$$\lambda_i(s) = \frac{1/\rho}{s^2 + \omega_i^2} \qquad [8b]$$

Based on Eqs. [6a-c] and [8a-b], the plant shown in Fig. 6 may be redrawn as shown in Fig. 8 which is a modal expansion of the distributed plant.

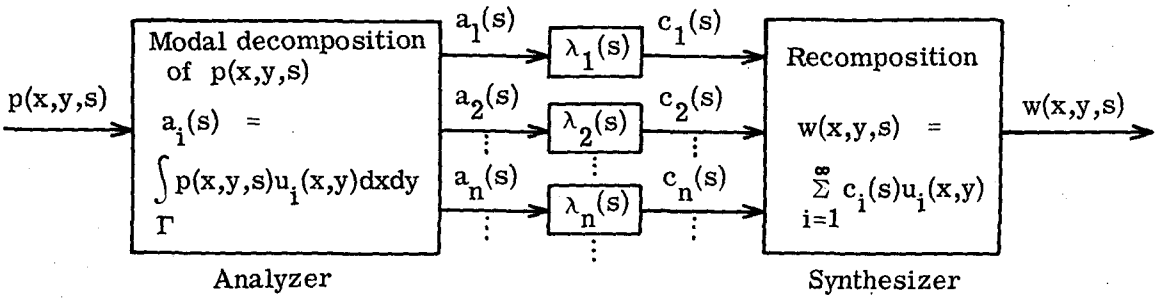

Figure 8.- Modal representation of the plant.

More generally, Fig. 6 represents the functional equation

$$w(z,t) = Lp(z,t) \qquad [9]$$

where z represents a general spatial variable (in one or more dimensions) and the operator L operates on functions of time and distance. Laplace transforming Eq. [9] with respect to time yields

$$w(z,s) = Lp(z,s) \qquad [10]$$

where the eigenvalues of L satisfy

$$Lu_i(z) = \lambda_i(s)u_i(z). \qquad [11]$$

Since the $u_i(z)$ are assumed to form a complete set, the separable functions $w(z,s)$ and $p(z,s)$ can be expanded as

$$w(z,s) = \sum_{i=1}^{\infty} c_i(s)u_i(z) \qquad [12a]$$

and

$$p(z,s) = \sum_{i=1}^{\infty} a_i(s)u_i(z). \qquad [12b]$$

Substituting [11], [12a], and [12b] into [10] yields

$$\sum_{i=1}^{\infty} c_i(s)u_i(z) = L \sum_{i=1}^{\infty} a_i(s)u_i(z) = \sum_{i=1}^{\infty} a_i(s)\lambda_i(s)u_i(z) \qquad [13a]$$

and consequently,

$$c_i(s) = \lambda_i(s)a_i(s) \qquad [13b]$$

with $a_i(s)$ defined by the transform of Eq. [6c]. Figure 8 is then the general modal representation of the class of distributed plants under investigation. In a function space where the eigenfunctions of L are used as the coordinates the system is represented by the infinite diagonal matrix

$$\Lambda(s) = \left[\lambda_i(s)\right]. \qquad [14]$$

In this reference frame, control of the plant output can be readily achieved by individually compensating each element of the diagonal matrix, as shown in Fig. 9.

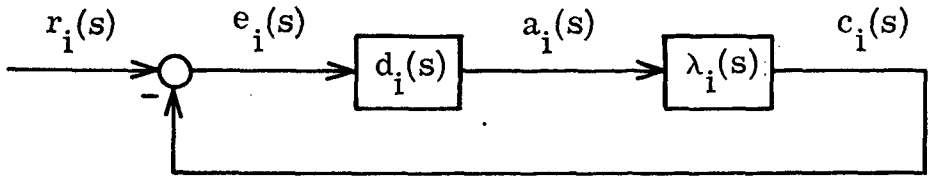

Figure 9.- Decoupled compensation of $\lambda_i(s)$.

The significance of the modal control indicated in Fig. 9 is that it is relatively easy to express the system least squares performance in terms of the orthonormal modes of a vibrating structure. This is a phenomenon of particular interest in the mirror application since the integral square error is the desired performance index of an optical surface.[12] With the error in the optical surface w_e represented by the modal coefficients e_i the image index (expected integral square error) is given by

$$J_I = E\left[\int_\Gamma w_e^2(z,t)dz\right] = E\left\{\int_\Gamma \left[\sum_{i=1}^{\infty} e_i(t)u_i(z)\right]^2 dz\right\}$$

$$= E\left[\sum_{i=1}^{\infty} e_i^2(t)\right] = \sum_{i=1}^{\infty} \sigma_{e_i}^2 \qquad [15]$$

where E denotes the expectation and $\sigma_{e_i}^2$ is the variance of the error in the i^{th} mode which is assumed to have a zero mean. The last steps result since $u_i(z)$ is a member of an orthonormal set. Thus, the measure of image quality, J_I, is a simple function of the variance of the mode

error which can be reduced by appropriate control one mode at a time as indicated in Fig. 9. Relating the original signals in the system to those of the decoupled reference frame, the control system structure becomes that shown in Fig. 10 where e and a are column matrices whose elements are the modal coefficients e_i and a_i, respectively. In practice the situation illustrated in Fig. 10 can only be approximated. The function of the analyzer is to determine the modal content of the optical surface error. The decoupled controller dynamics, represented by the matrix $D(s) = \text{diag}\left[d_i(s)\right]$, is determined on the basis of standard design techniques (see Fig. 9) to achieve a satisfactory performance level. For a well-ground mirror the need for corrective action diminishes as the mode number, i, increases and control can be reasonably be restricted to the significant modes. The N controlled modes are denoted by the output and error N vectors c^N and e^N in Fig. 11. The finite $(N \times N)$ controller matrix is represented by D^N. The function of the load synthesizer is to place an appropriate force distribution on the plate to correct for the modal errors in e^N. Since the remaining modes are unmonitored (no corrective action taken), the ideal force distribution applied by the loading mechanism is

$$p_{ideal}(z,t) = \sum_{i=1}^{N} a_i(t)\, u_i(z) \qquad [16]$$

with none of the uncontrolled modes excited. Physically this corrective loading is applied by finite number of control manipulators which, in

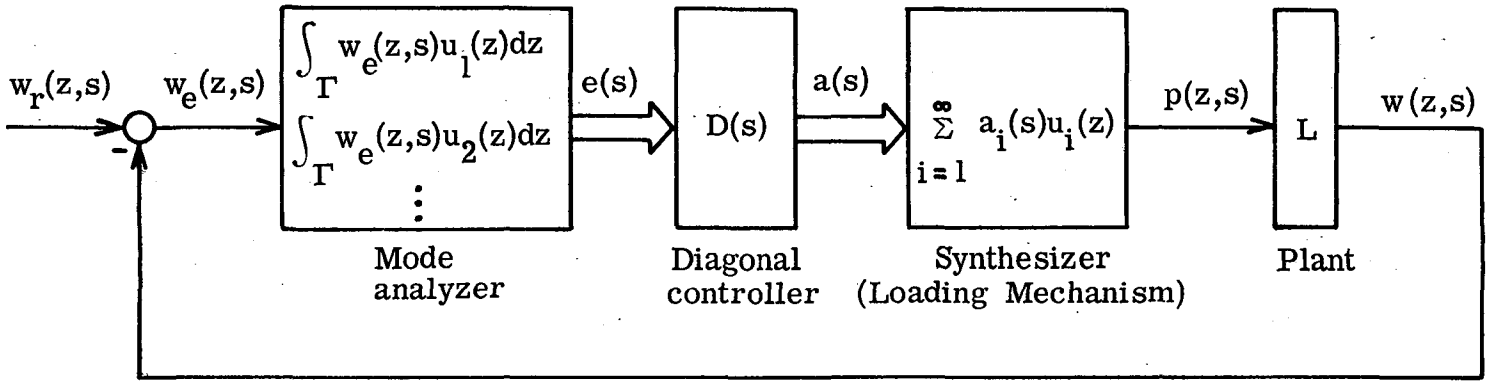

Figure 10.- Controller representation in the original reference frame.

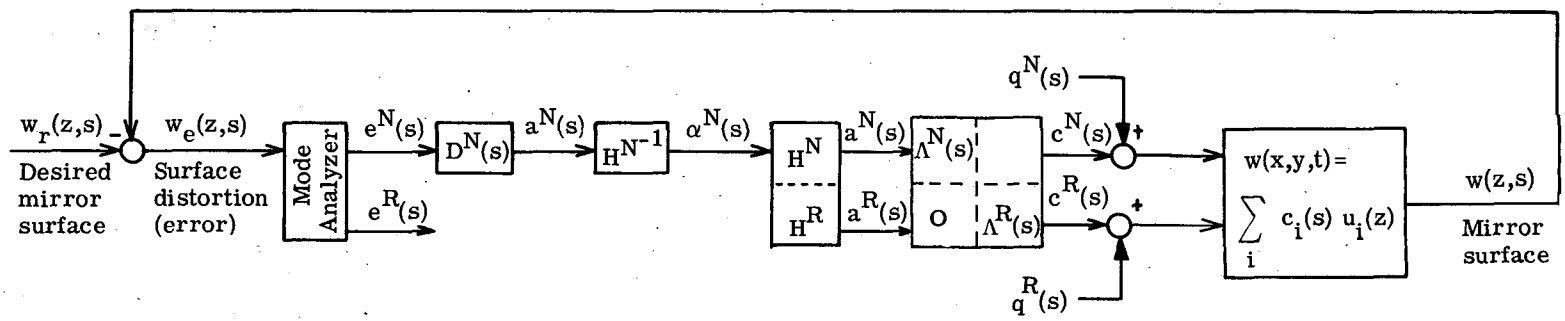

Figure 11.- Partitioned representation of the controller and plant.

the mirror problem, are comprised of displacement actuators in series with a spring acting against a backing structure. The spring is attached to the mirror by means of a pad intentionally introduced to restrict the excitation of uncontrolled modes (a point discussed in detail later in the paper). The actual (non-ideal) force density applied by these N actuators is given by

$$p(z,t) = \sum_{j=1}^{N} p_j(z,t) = \sum_{j=1}^{N} \alpha_j(t)\beta_j(z) \qquad [17]$$

where p_j represents the force distribution resulting from the j^{th} actuator, and the last step results under the assumption that each applied force distribution is separable in time and distance. Expanding each of the $\beta_j(z)$ in terms of the eigenfunctions, $u_i(z)$, Eq. [17] becomes

$$p(z,t) = \sum_{i=1}^{\infty} \left[\sum_{j=1}^{N} h_{ij}\alpha_j(t) \right] u_i(z) \qquad [18a]$$

where

$$h_{ij} = \int_{\Gamma} \beta_j(z)u_i(z)dz \qquad [18b]$$

and comparison with [6b] reveals

$$a_i(t) = \sum_{j=1}^{N} h_{ij}\alpha_j(t). \qquad [19a]$$

In matrix form this relation between the mode force coefficients and the actuator signals becomes

$$a = H\alpha^N \qquad [19b]$$

where H is an ∞ x N matrix and α^N is an N vector. Equation [19b] indicates the control elements excite all modes. Since only N of the more significant modes are controlled, Eq. [19b] is partitioned as

$$\begin{bmatrix} a^N \\ \hline a^R \end{bmatrix} = \begin{bmatrix} H^N \\ \hline H^R \end{bmatrix} \begin{bmatrix} \alpha^N \end{bmatrix} \qquad [20]$$

where H^N is an N x N matrix, H^R an ∞ x N matrix, a^N an N vector corresponding to the controlled modes, and a^R accounts for the remaining modal force coefficients. To provide the desired corrective vector a^N the actuator inputs are given by

$$\alpha^N = \left[H^N\right]^{-1} a^N \qquad [21]$$

where it is assumed that the actuator locations insure H^N is non-singular - this point is discussed in detail in a subsequent section. Partitioning the matrix representing the plant dynamics into components corresponding to the controlled and uncontrolled modes, the overall system becomes that shown in Fig. 11 where disturbances q^N and q^R acting on the plant are included as equivalent displacements. When the mode number, i, is ordered with increasing frequency of vibration, $\omega_i = \omega_{mn}$, the plant inherently performs modal filtering which attenuates the

higher modes so that their contribution to the error (mirror distortion) rapidly becomes negligible as the mode number increases. Consequently, it is often assumed that only the first N modes are present, i.e., c^R and a^R are identically zero, and considerable simplification results. For example, let w^N be an N vector defined by the output at N different points. That is,

$$w^N = \text{col } w(z_j,t) \qquad [22]$$

where z_j represents a measurement point. In terms of the mode displacement coefficients

$$w^N = U^N c^N \qquad [23a]$$

where

$$U^N = \begin{bmatrix} u_1(z_1) & u_2(z_1) & \cdots & u_N(z_1) \\ u_1(z_2) & u_2(z_2) & \cdots & u_N(z_2) \\ \vdots & \vdots & & \vdots \\ u_1(z_N) & u_2(z_N) & \cdots & u_N(z_N) \end{bmatrix} . \qquad [23b]$$

Under these conditions the mode analyzer becomes simply an operation on the N measurements; specifically

$$c^N = \left[U^N\right]^{-1} w^N \qquad [24]$$

where the sensors are located at positions to insure U^N is nonsingular. The control structure of Fig. 11 then reduces to the N × N multivariable

system[2] shown in Fig.12. This idealized representation, valid when the effects of the higher modes can be safely neglected, was derived by Gould and Murray-Lasso and is treated in detail in reference 1. Control of the low-order high-amplitude modes as indicated in Fig. 12, or in the decoupled form of Fig. 9, presents the classic problem[13] of controlling a resonant plant with a limited control effort (restricted actuator throw). While for large primary mirrors with low resonant frequencies this may be a substantial problem, in the present paper it is assumed that the disturbances $q^N(t)$ are slowly varying and of sufficiently small amplitude that any desired degree of control can be realized. Negligible contribution from the uncontrolled modes can generally be assured by permitting N to be arbitrarily large. However, in the present problem extremely accurate control of the optical surface of the thin deformable mirror for diffraction-limited performance is required with a minimum number of actuators. Under these conditions the effects of e^R and a^R are not negligible, but, in fact, represent the most significant system errors and the most important factors in evaluating design tradeoffs.

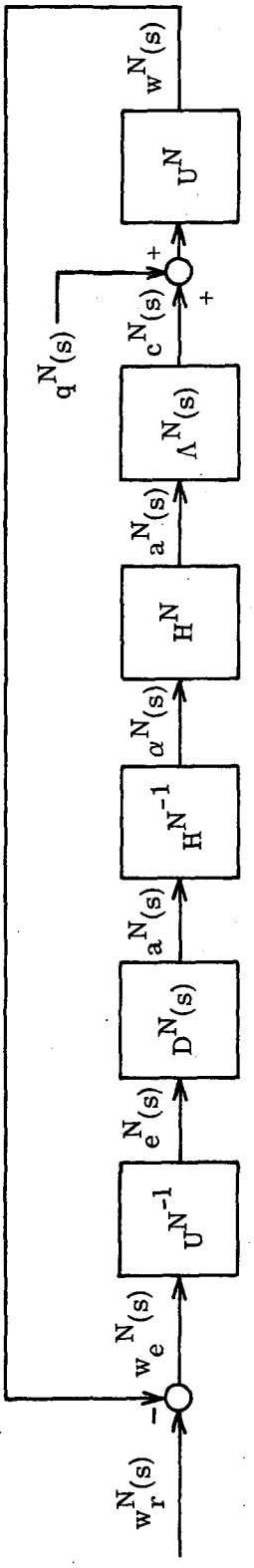

Figure 12.- Idealized N × N multivariable system resulting from a finite modal expansion of the distributed system.

III. ACTUATOR PAD SIZE AND LOCATION AS DESIGN FACTORS

The uncontrolled modes enter the problem in two major ways. First, the actuators excite not only the controlled modes but, in general, all modes. To demonstrate, first separate the image quality index into two parts, i.e.,

$$J_I = J_N + J_R \qquad [25a]$$

where

$$J_N = \sum_{i=1}^{N} \sigma_{e_i}^2 \qquad [25b]$$

accounts for the error in the controlled modes and

$$J_R = \sum_{i=N+1}^{\infty} \sigma_{e_i}^2 \qquad [25c]$$

accounts for the remnant error of uncontrolled modes. As larger actuator displacements are commanded in order to reduce J_N to smaller and smaller values J_R increases due to the effect of a^R. Secondly, unless direct measurements of the modes are made, a limitation on the ability of the displacement sensors to obtain an uncorrupted estimate of the N controlled modes results from the presence of e^R.

Actuator Pad Size

The function of the actuators, as indicated in the previous section, is to apply forces to reduce e^N while minimizing the excitation of the uncontrolled modes, i.e., ideally

$$H = \begin{bmatrix} H^N \\ \hline 0 \end{bmatrix}, \quad H^N \text{ nonsingular.} \qquad [26]$$

In the mirror problem the control manipulators are modeled by a displacement actuator working against a backing plate and a relatively soft spring which is attached to the mirror by means of a pad. The ability to approach the situation on Eq. [26] is governed by pad size and location, which are factors under the influence of the designer. To illustrate the effect of pad size, consider the rectangular plate of Fig. 7. The pads are assumed to be rectangular in shape and located as shown in Fig. 13.

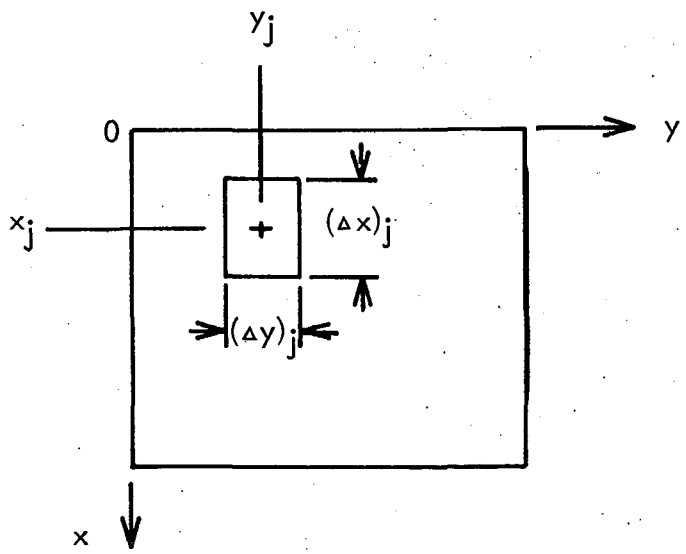

Figure 13.- Pad shape, size, and location.

The amount of force applied by the j^{th} actuator is determined by the product of the spring constant K and displacement actuator position. This force loads the plate as indicated by Eq. [17] with

$$\beta_j(x,y) = \frac{Kf_j(x,y)}{\iint_\Gamma f_j(x,y)dx\,dy} \qquad [27]$$

where $f_j(x,y)$ is the distribution of the force and $\alpha_j(t)$ is the control input. Considering a force distribution that is constant over the area of the pad, Eq. [18b] yields

$$h_{ij} = \frac{K}{(\Delta x)_j(\Delta y)_j} \int_{\substack{j^{th}\ pad\\ area}} \int \frac{4}{ab} \sin\frac{m\pi x}{a} \sin\frac{n\pi y}{b}\,dx\,dy$$

$$= \frac{4K}{ab} \sin\frac{m\pi x_j}{a} \sin\frac{n\pi y_j}{b} \left[\frac{\sin\frac{m\pi(\Delta x)_j}{2a}}{\frac{m\pi}{2a}(\Delta x)_j} \cdot \frac{\sin\frac{n\pi(\Delta y)_j}{2b}}{\frac{n\pi}{2b}(\Delta y)_j} \right] \qquad [28]$$

where i indexes the mode m,n. For this special case with constant pad size (i.e., $(\Delta x)_i = (\Delta x)_j = \Delta_a$ and $(\Delta y)_i = (\Delta y)_j = \Delta_b$), Eq. [28] may be rewritten in matrix form as

$$H = GU' \qquad [29a]$$

where U is the N x ∞ matrix,

$$U = \begin{bmatrix} u_1(z_1) & u_2(z_1) \cdots u_i(z_1) \cdots \\ \vdots & \vdots \quad \vdots \quad \vdots \\ u_1(z_N) & u_2(z_N) \cdots u_i(z_N) \cdots \end{bmatrix}, \qquad [29b]$$

the prime denotes the transpose of a matrix, z_i denotes the point x_i, y_i,

$$G = \text{diag } g_i(\Delta_a, \Delta_b) , \qquad [29c]$$

and

$$g_i = g_{mn} = K \begin{bmatrix} \dfrac{\sin \dfrac{m\pi\Delta_a}{2a}}{\dfrac{m\pi\Delta_a}{2a}} & \dfrac{\sin \dfrac{n\pi\Delta_b}{2b}}{\dfrac{n\pi\Delta_b}{2b}} \end{bmatrix} . \qquad [30]$$

Figure 14 contains a plot of $(\sin \xi)/\xi$. Assuming the controlled modes are $m \leq m_{max}$ and $n \leq n_{max}$ and pad dimensions are $\Delta_a \leq \frac{a}{m_{max}}$ and $\Delta_b \leq \frac{b}{n_{max}}$, the maximum value of the argument for one of the controlled modes is $\xi = \pi/2$ which occurs when adjacent pads touch. The attenuation of the higher order modes by the pad is apparent from this diagram as the elements of G decrease rapidly for $i > N$ and, in turn, decrease the output levels of H^R approaching the idealized condition of Eq. [26].

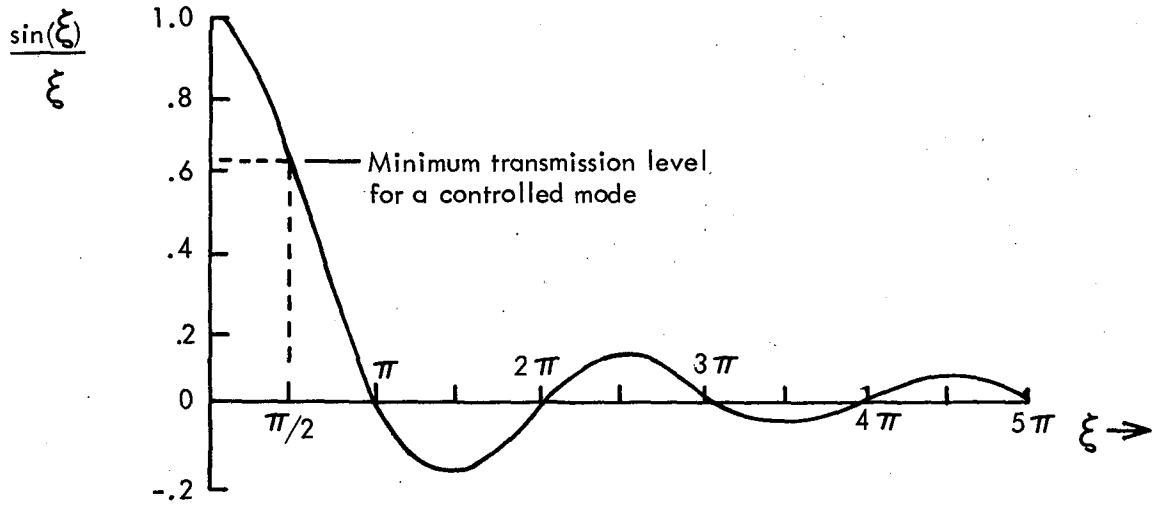

Figure 14.- Plot of sin $(\xi)/\xi$ illustrating the filtering action of pad.

The prefilter action of the pad is complemented by the transmission properties of the plate itself. For the rectangular plate of Fig. 6 the relation between the applied loading and displacement output for the i^{th} mode is

$$c_i(s) = \frac{a_i(s)/\rho}{s^2 + \epsilon s + \omega_i^2} \qquad [31]$$

where a small amount of damping has been included. In response to a step input the steady transmission is

$$\lim_{t \to \infty} \frac{c_i}{a_i} = \frac{1}{\rho \omega_i^2} \qquad [32]$$

where ω_i^2 is given by Eq. [5a]. Assuming a 0.5 inch (1.27 cm) thick, 30-inch (76.2 cm) square plate with a Young's modulus of 10^7 pounds per square inch (70.3×10 gm/cm^2) and a Poisson's ratio of 0.2, this factor is

$$\lim_{t \to \infty} \frac{c_i}{a_i} = \frac{7.73 \times 10^{-2}}{(m^2 + n^2)^2} . \qquad [33]$$

A byproduct of the pad's desired effect on H^R is a decrease in the transmission properties of H^N. As a consequence, an increased effort is required to deflect the surface. This is readily demonstrated for the simply supported rectangular plate where

$$H^N = G^N U^{N'} \qquad [34]$$

and with appropriate actuator placement U^N is orthonormal (see Appendix B). Consider the expected value of the norm of the actuator displacement vector given by

$$\alpha^{N'} \alpha^N = \left[a^{N'}\right]\left[G^{N'}\right]^{-1}\left[G^N\right]^{-1} a^N = \sum_{i=1}^{N} \left(\frac{\sigma_{a_i}}{g_i}\right)^2 . \qquad [35]$$

Thus, as the elements of G^N are decreased, the required control displacement and force increases. Since the plate itself was shown to perform substantial filtering, a compromise on the final pad shape and size is normally employed.

Actuator Location

Another critical factor on the H^N and H^R matrices is the placement of the actuators. The actuator locations must be selected to prevent the occurrence of a singular H^N matrix. Since the actuator locations most directly affect the U^N matrix, knowledge of the mode shapes will generally permit the selection of the location of the actuators. This situation is detailed in the examples. Evaluation of the determinant may be used to verify the invertibility of H^N. In addition, if a row of H^R is zero, the mode corresponding to that row cannot be excited. This is approximately achieved for most plants by locating pads at the zeros (nodes) of the mode in question. For the rectangular plate, this is exactly achieved since the influence of pad location of H is delineated by U', see Eq. [29]. When the modes are ranked in order of importance, the desired goal is to control the first N and null the next highest modes; however, this is not usually possible and trade-offs are required. For example, it may be possible to control a set of modes that are not the N most significant but be able to preclude excitation of the next highest modes or, alternatively, control the N most significant modes but not have the ability to preclude excitation of the most dominant uncontrolled modes. Since the controlled modes may be reduced to any desired level at the cost of some increase in the amplitudes of the unmonitored modes, the contribution of these higher modes to system error represents the most critical factor in system design. Determination of the trade-offs in actuator size and placement

is obtained through evaluation of the system performance index, J_I, which is discussed below and illustrated later in two examples.

IV. STATIC PERFORMANCE

The design objective is to minimize the image index defined as the expectation of the integral square surface error. As shown in Eq. [15] this is a function of the mean square values of the modal error coefficients. Determination of J_I as given by Eqs. [25a-c] is dependent on the nature, particularly the spectral content, of the disturbances. For the application to the control of a deformable primary mirror of an orbiting telescope, it is anticipated that the primary error sources will be initial figuring errors and relatively slowly time-varying thermal gradients. In this context it is reasonable to expect that the system will generally be performing at or near its static values.

In Fig. 11 the surface deformation due to the disturbances is defined in terms of its displacement modal expansion coefficients, q. No loss in generality results from considering the disturbances to be displacements since equivalent force distributions could be assumed. With reference to Fig. 11, and with $\omega_r(z,s)$ zero, the error in the control modes is given by

$$e^N = - \left[I + \Lambda^N D^N \right]^{-1} q^N. \qquad [36]$$

For the static situation this reduces to

$$e_i = \frac{-1}{1 + K_i} q_i \qquad 0 < i \leq N \qquad [37]$$

where K_i is the loop gain (type 0 system) for the i^{th} mode. When the loop transmission contains a pure integration (type 1 system), $K_i \to \infty$. Thus the error in the controlled modes can theoretically be reduced to any arbitrarily small value. The expected value for J_N then becomes

$$J_N = \sum_{i=1}^{N} \left(\frac{1}{1 + K_i} \right)^2 \sigma_{q_i}^2 \qquad [38]$$

where σ_{q_i} is the rms value of the static (or slowly varying) disturbance. The error in the uncontrolled modes is given by

$$\begin{aligned} e^R &= - q^R - \Lambda^R H^R \alpha^N \\ &= - q^R + \Lambda^R H^R \left[H^N \right]^{-1} D^N \left[I + \Lambda^N D^N \right]^{-1} q^N \end{aligned} \qquad [39]$$

which under static conditions becomes

$$e_i = - q_i + \sum_{j=1}^{N} \psi_{ij} \frac{K_j}{1 + K_j} q_j \qquad N + 1 \leq i \qquad [40a]$$

where ψ_{ij} is an element of the matrix

$$\psi = \Lambda^R H^R \left[\Lambda^N H^N \right]^{-1}. \qquad [40b]$$

Assuming the modal coefficients of the disturbance are uncorrelated, i.e.,

$$E(q_i q_j) = \begin{cases} 0 & i \neq j \\ \sigma_{q_i}^2 & i = j \end{cases} \qquad [41]$$

the expected error in the uncontrolled modes becomes

$$J_R = \sum_{i=N+1}^{\infty} \sigma_{q_i}^2 + \sum_{j=N+1}^{\infty} \left[\sum_{i=1}^{N} \psi_{ji}^2 \left(\frac{K_i}{1+K_i} \right)^2 \sigma_{q_i}^2 \right] = J_{R_o} + J_{R_c} \qquad [42]$$

where J_{R_o} is the value of the disturbance error in the higher modes without control. The second term J_{R_c} is clearly positive and represents the increase in J_R that results from the actuator displacements required to control the errors in the first N modes. Since J_{R_c} is finite, the series converges and the order of summation may be reversed, yielding

$$J_R = J_{R_o} + \sum_{i=1}^{N} \varphi_i^2 \left(\frac{K_i}{1 + K_i} \right)^2 \sigma_{q_i}^2 \qquad [43a]$$

where

$$\varphi_i^2 = \sum_{j=N+1}^{\infty} \psi_{ji}^2 \qquad [43b]$$

is a constant dependent on the design factors of actuator pad size and location as well as the natural modal filtering performed by the plant. Combining Eqs. [25a-c], [38], and [43] yields as the imaging index

$$J_I = J_{R_o} + \sum_{i=1}^{N} \left[\left(\frac{1}{1 + K_i} \right)^2 \sigma_{q_i}^2 + \left(\frac{\varphi_i K_i}{1 + K_i} \right)^2 \sigma_{q_i}^2 \right]. \qquad [44]$$

The first term is unaffected by the control action, the second decreases as a result of the control action and the third increases.

Since J_{R_o} is constant, minimization of Eq. [44] with respect to K_i yields optimum performance when

$$K_i = \frac{1}{\varphi_i^2} \qquad [45]$$

and

$$J_{I_{opt}} = \sum_{i=1}^{N} \left(\frac{1}{1 + K_i}\right) \sigma_{q_i}^2 + J_{R_o} = \sum_{i=1}^{N} \frac{\varphi_i^2}{1 + \varphi_i^2} \sigma_{q_i}^2 + J_{R_o} \qquad [46]$$

with the controlled and uncontrolled components given by

$$J_{N_{opt}} = \sum_{i=1}^{N} \left(\frac{1}{1 + K_i}\right) \sigma_{q_i}^2 = \sum_{i=1}^{N} \left(\frac{\varphi_i^2}{1 + \varphi_i^2}\right) \sigma_{q_i}^2 \qquad [47]$$

and

$$J_{R_{opt}} = \sum_{i=1}^{N} \frac{K_i}{(1 + K_i)^2} \sigma_{q_i}^2 + J_{R_o} = \sum_{i=1}^{N} \frac{\varphi_i^2}{(1 + \varphi_i^2)^2} \sigma_{q_i}^2 + J_{R_o}. \qquad [48]$$

Recalling that without control $J_{N_o} = \sum_{i=1}^{N} \sigma_{q_i}^2$, it is seen that for large loop gain the error in each term of $J_{R_{opt}}$ due to control is approximately $1/K_i$ while each term in $J_{N_{opt}}$ is reduced by an additional $1/K_i$. Thus, if significant improvement is to be gained in the optical surface by the above method, N must be selected sufficiently large and the actuator size and placement such that $\varphi_i^2 = 1/K_i \ll 1$. In the mirror

situation J_{R_o} is negligible and J_{R_c} represents the major source of concern.

Because K_i is large, a type 1 system is normally employed and

$$J_I = \sum_{i=1}^{N} \varphi_i^2 \sigma_{q_i}^2 + J_{R_o}. \qquad [49]$$

The required value of N to achieve the desired rms figuring error can be minimized by the selection of pad size and location whose effect is manifest through the parameters φ_i^2.

V. MODE ESTIMATION ERROR

The preceding analysis assumed ideal measurement of the controlled modal variables e_i; however, in many applications it is neither practical nor possible to obtain direct measurements. In these cases an estimate is often derived from a spatial sampling of the distributed output. This is the case in the mirror problem where the most commonly used measurement of the optical surface is performed by the interference method illustrated in Fig. 15. This mirror figure error sensor is a modified form of a Twyman-Green interferometer. In this interferometer two plane wavefront beams are formed from a common coherent source. One beam is reflected from a reference flat while the second is converted to a spherical wavefront whose center of curvature is that of the mirror. This wavefront is returned by the mirror and forms an interference pattern with the reference beam which is focused on the N discrete individual sensors. Periodic motion of the reference flat produces a sine wave of identical frequency at each detector. This converts the error determination from an amplitude to a phase measurement and permits the required sensitivity to be achieved.

Under conditions where no modes except the first N exist, the relation of the modal coefficients to the N measured values is given by Eq. [24] which for the mode error is

$$e^N_{meas} = \left[U^N\right]^{-1} w^N_e. \qquad [50]$$

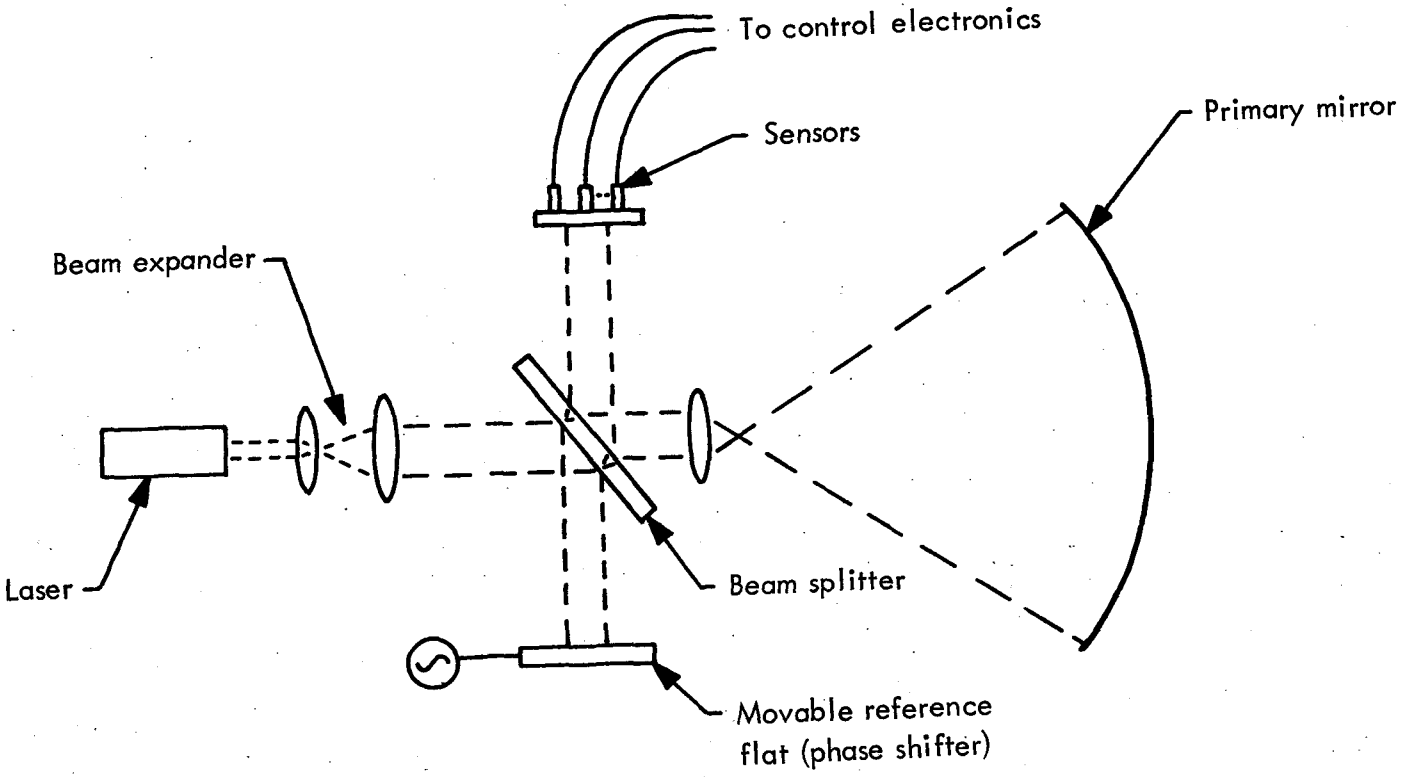

Figure 15.- Schematic of the mirror figure error sensor.

However, the presence of the high-order modes deteriorates this measurement since the actual measured vector is defined by

$$w_e^N = U^N e^N + U^R e^R \qquad [51]$$

where U^R is the N x ∞ matrix

$$U^R = \begin{bmatrix} u_{N+1}(z_1) & \cdots & u_{N+j}(z_1) & \cdots \\ \vdots & \ddots & \vdots & \\ u_{N+1}(z_N) & \cdots & u_{N+j}(z_N) & \cdots \end{bmatrix}. \qquad [52]$$

Consequently, the estimate of the modes in Eq. [50] becomes

$$e^N_{meas} = \left[U^N\right]^{-1} U^N e^N + \left[U^N\right]^{-1} U^R e^R = e^N + \epsilon^N \qquad [53]$$

The manner in which the measurement error ϵ^N, defined in Eq. [53], evolves is shown in Fig. 16. The disturbance error in the first N modes can be controlled to an arbitrarily small value (see Eq. [38]), while errors in the remaining modes cannot be counteracted. A major effect of the measurement error in Eq. [53] is to introduce an additional error in the controlled modes. To illustrate, the vector e^N is seen from Fig. 16 to be given by

$$e^N = -\Lambda^N H^N \alpha^N - q^N \qquad [54a]$$

where

$$\alpha^N = \left[H^N\right]^{-1} D^N \left[e^N + \epsilon^N\right], \qquad [54b]$$

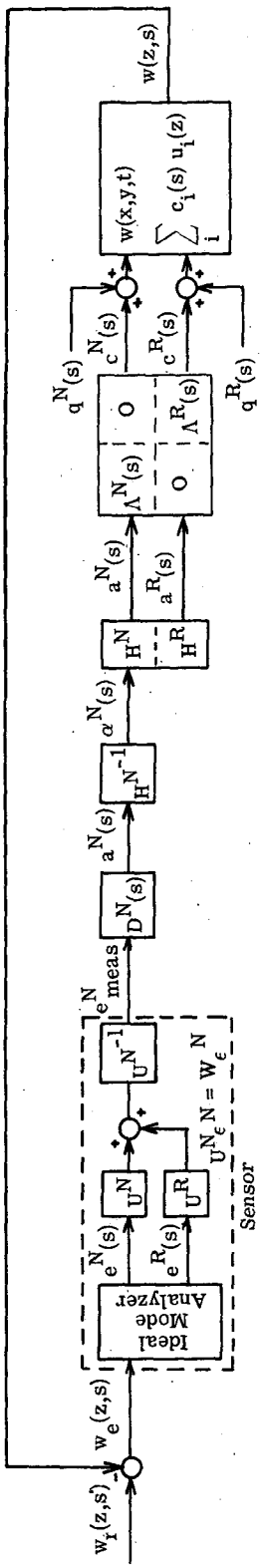

Figure 16.- System configuration including measurement errors.

and substituting [54b] into [54a] and rearranging yields

$$e^N = -\left[I + \Lambda^N D^N\right]^{-1} q^N - \left[I + \Lambda^N D^N\right]^{-1} \Lambda^N D^N \epsilon^N. \qquad [55]$$

For a type 0 system under static conditions, Eq. [55] becomes

$$e_i = -\frac{q_i}{1 + K_i} - \frac{K_i}{1 + K_i}\epsilon_i \qquad i \leq N \qquad [56a]$$

or, for a type 1 system

$$e^N = -\epsilon^N = -\left[U^N\right]^{-1} U^R e^R. \qquad [56b]$$

Attention is now given to the error defined by Eq. [56b] since, as previously established, most practical systems would possess an infinite loop gain. Two distinct cases are now considered: one where e^R is dominated by the disturbances acting on the plant, i.e.,

$$e^R = -q^R \qquad [57]$$

and, secondly, where the error in the higher-order modes contributed by the disturbance vector, q^R, is negligible but the error introduced by the control effort is significant, i.e.,

$$e^R = -\Lambda^R H^R \alpha^N = +\Lambda^R H^R \left[\Lambda^N H^N\right]^{-1} (q^N - \epsilon^N)$$

$$= (I + \psi\left[U^N\right]^{-1} U^R)^{-1} \psi q^N. \qquad [58]$$

For ease in later calculations it is assumed that $\psi\left[U^N\right]^{-1} U^R$ is negligible compared to I and that U^N is nearly orthogonal permitting the contribution

to J_N arising from ϵ^N to be determined from the norm of the measurement error at the N measurement points $w_\epsilon^N = U^R e^R = U^N \epsilon^N$. That is,

$$J_{N_{meas}} = E\left[\epsilon^{N'}\epsilon^N\right] = E\left[w_\epsilon^{N'} w_\epsilon^N\right] \qquad [59a]$$

where

$$w_\epsilon^N = \begin{cases} - U^R q^R & \text{case I} \\ - U^R{}_\psi q^N & \text{case II} \end{cases}. \qquad [59b]$$

If the modal coefficients of the disturbances are uncorrelated then Eq. [59a] for case I becomes

$$J_{N_{meas}} \cong E\left[w_\epsilon^{N'} w_\epsilon^N\right] = \sum_{i=N+1}^{\infty} \left[\sum_{n=1}^{N} u_i^2(z_n)\right] \sigma_{q_i}^2. \qquad [60]$$

The sensor locations are chosen to minimize $\sum_{n=1}^{N} u_i^2(z_n)$ for as many of the more significant high order modes as possible. This result is consistent with that concluded with regard to actuator placement and, consequently, the criteria for actuator and sensor placement are identical. Since increasing the number of sensors is relatively inexpensive, in many cases it will be desirable to have more sensors than actuators (or controlled modes). If $M > N$ sensors are used, a parallel development indicates that with increased measurements

$$J_{N_{meas}} \cong \sum_{i=M+1}^{\infty} \left[\sum_{n=1}^{N} u_i^2(z_n)\right] \sigma_{q_i}^2 \qquad [61]$$

yielding an expected improvement of

$$\Delta J_{N_{meas}} = \sum_{i=N+1}^{M} \left[\sum_{n=1}^{N} u_i^2(z_n) \right] \sigma_{q_i}^2 . \qquad [62]$$

For the second case, of which the mirror problem is typical, the distortion in the higher modes is caused by the control action and the measurement error at the n^{th} sample point is

$$w_\epsilon(z_n) = \sum_{i=N+1}^{\infty} \left[\sum_{j=1}^{N} u_i(z_n)\psi_{ij} \right] q_j . \qquad [63]$$

From the properties of the disturbances, the expected value of $w_\epsilon^2(z_n)$ can be determined and is given by

$$E\left[w_\epsilon^2(z_n)\right] = \sum_{i=1}^{N} \left[\sum_{j=N+1}^{\infty} u_j(z_n)\psi_{ji} \right]^2 \sigma_{q_i}^2 \qquad [64a]$$

and

$$J_{N_{meas}} \cong \sum_{n=1}^{N} w_\epsilon^2(z_n) = \sum_{i=1}^{N} \left\{ \sum_{n=1}^{N} \left[\sum_{j=N+1}^{\infty} u_j(z_n)\psi_{ji} \right]^2 \right\} \sigma_{q_i}^2 . \qquad [64b]$$

This error is on the order of magnitude of the error in the uncontrolled modes J_R and represents the effect of estimating the modal coefficients from output measurements. Increasing the number of sensors, as suggested, will substantially reduce this error if the remnant J_R is dominated by the first few higher modes.

VI. SUMMARY OF DESIGN CONSIDERATIONS

The performance index for the system is broken into two parts: (1) that contributed by the controlled modes, and (2) that due to the uncontrolled modes. Application of active control reduces the error in the controlled modes to any arbitrary level while the disturbances producing errors in the (uncontrolled/unmonitored) higher modes cannot be counteracted. Further, the corrective forces applied by the finite number of discrete actuators excites additional errors in the higher modes. When mode estimation is employed, errors due to measurement uncertainty are introduced into the first N modes. Thus, the total system error is given by

$$J_I = J_{N_{meas}} + J_{R_o} + J_{R_c} \qquad [65]$$

where $J_{N_{meas}}$, J_{R_o}, and J_{R_c} are defined in Eqs. [59a] and [42]. It was observed that these errors may be minimized by factors under the designer's control. These factors are actuator location, pad size, and sensor location. Selection of actuator location permitted minimization of the excitation of the more significant uncontrolled modes. The pad size was seen to act as a filter which attenuates the effect of the control input in exciting the higher modes. The pad size is selected to cause the modal content of the applied force loading to drop off quickly above the N^{th} mode. Combined with actuator locations that minimally excite the first few (most significant) higher modes, the pads together with the plant provide the desired modal filtering for the

remaining high-order modes. Finally, if estimation errors are to be minimized, sensor location requirements become the same as those for actuator placement. In some instances, additional sensors may be used to reduce the errors in estimating the modal coefficients.

The above points are illustrated most clearly by the example of a simply supported, thin, square, flat plate with the following parameters:

Thickness	0.5 inch (1.27 cm)
Length	30 inches (76.2 cm)
Width	30 inches (76.2 cm)
Young's modulus	10^7 psi (70.3×10^7 gm/cm^2)
Poisson's ratio	0.2

Table 1 contains values of ω_i^2 which are inversely proportional to mode transmission as given by the steady values of the Λ matrix. The modes are ranked, from most to least significant, in terms of decreasing $(1/\omega_i)^2$ and control of the low-order modes is desired. With the modes ordered with m on the ordinate and n on the abscissa, contours of equal $(\omega_i)^2$ become circles in the n,m plane. These circles may be approximated by squares; for example, if 25 modes are to be controlled they would include $1 \leq n \leq 5$ and $1 \leq m \leq 5$ as shown in Fig. 17a. The next highest mode in each direction is $m = 6$ and $n = 6$ which has 25 mutual nodes equally spaced over the plate, see Fig. 17b. Actuator placement at these nodes (which can always be achieved since the m + 1 mode has m nodes) makes U^N orthogonal and precludes excitation of any mode for which m or n equal 6. Alternatively, the first N most significant modes may be controlled as illustrated in Fig. 17c. This is achieved by the actuator placement of Fig. 17d. The unexcited modes in the

m \ n	1	2	3	4	5	6	7	8	9	10
1	0.508	3.17	12.7	36.7	85.8	173.9	317.5	536.6	853.9	1295.5
2	3.17	8.13	21.5	50.8	106.8	203.2	356.7	587.2	917.5	1373.6
3	12.7	21.5	41.2	79.4	146.8	257.2	427.2	676.8	1028.7	1508.8
4	36.7	50.8	79.4	130.0	213.5	343.4	536.5	812.7	1194.9	1708.9
5	85.8	106.8	146.8	213.5	317.5	472.6	695.4	1005.9	1426.9	1984.3
6	173.9	203.2	257.2	343.4	472.6	658.3	917.5	1270.0	1738.5	2348.9
7	317.5	356.7	427.2	536.5	695.4	917.5	1219.7	1621.6	2146.2	2819.4
8	536.6	587.2	676.8	812.7	1005.9	1270.0	1621.6	2080.7	2670.1	3415.7
9	853.9	917.5	1028.7	1194.9	1426.9	1738.5	2146.2	2670.1	3332.9	4160.5
10	1295.5	1373.6	1508.8	1708.9	1984.3	2348.9	2819.4	3415.7	4160.5	5079.8

Table 1.- Values of ω^2_{mn} in 10^6 radians^2/seconds^2 for a flat square plate.

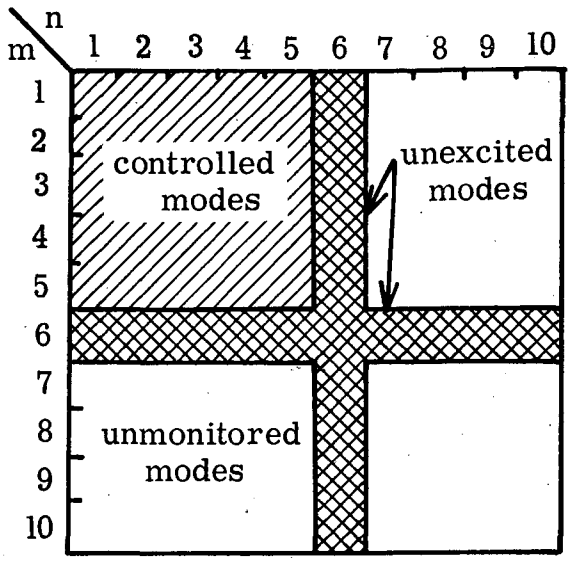

(a) The m,n plane for the actuator placement of b.

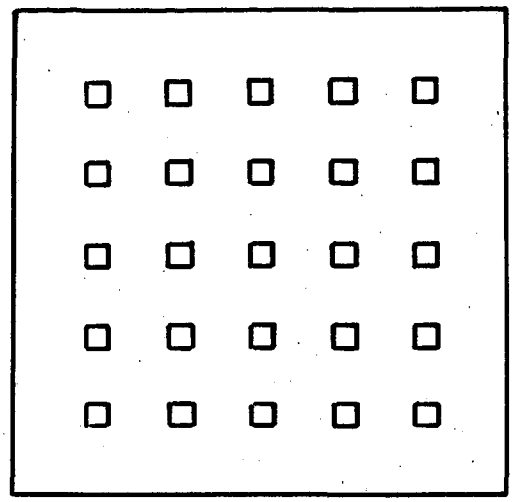

(b) An actuator configuration utilizing twenty-five actuators.

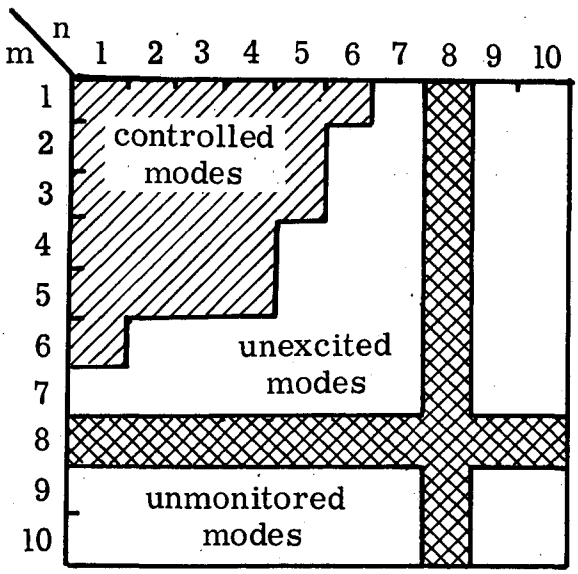

(c) The m,n plane for the actuator placement of d.

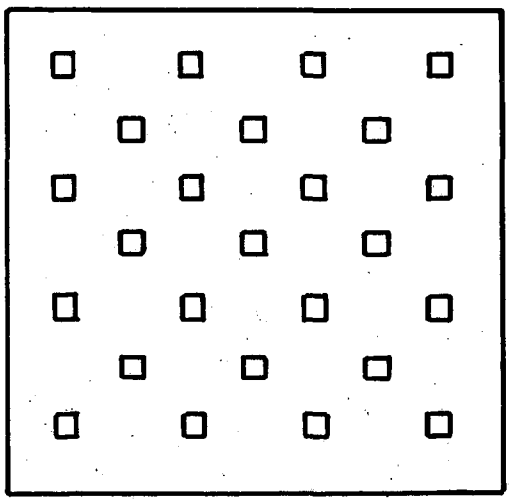

(d) An alternate actuator configuration utilizing twenty-five actuators.

Figure 17.- The locations in the m,n plane of the controlled, unexcited, and unmonitored modes of a flat rectangular plate.

latter case are those with m = 8 or n = 8. In any case, final determination of the optimal trade-off requires detailed evaluation of the performance index.

Since data regarding the disturbances to which a primary mirror surface is subjected are not presently available, a disturbance profile characterized by a modal force coefficient with a standard deviation of

$$\sigma_{a_i} = \frac{\sigma_{q_i}}{\lambda_i} = \frac{\sqrt{\text{plate area}}}{386.4} \qquad [66]$$

in pounds per square inch, for all i, was assumed. This profile yields an rms figure error of

$$F = \sqrt{\frac{J_I}{\text{plate area}}} \approx 50 \times 10^{-6} \text{ inches} \qquad [67]$$

for the uncontrolled surface which is in reasonable agreement with the figuring errors of the mirror whose diffraction pattern is given in Fig. 5. Pad size was selected to be 0.5 inches (1.27 cm) × 0.5 inches (1.27 cm). Fig. 18 displays the rms figuring error for a type 1 servo versus the number of actuators for placement of the type illustrated in Fig. 17b. The type 0 error was evaluated for optimal gain but did not provide a significant improvement for the error profile considered. The details of the procedure used to obtain Fig. 18 are contained in Appendix C.

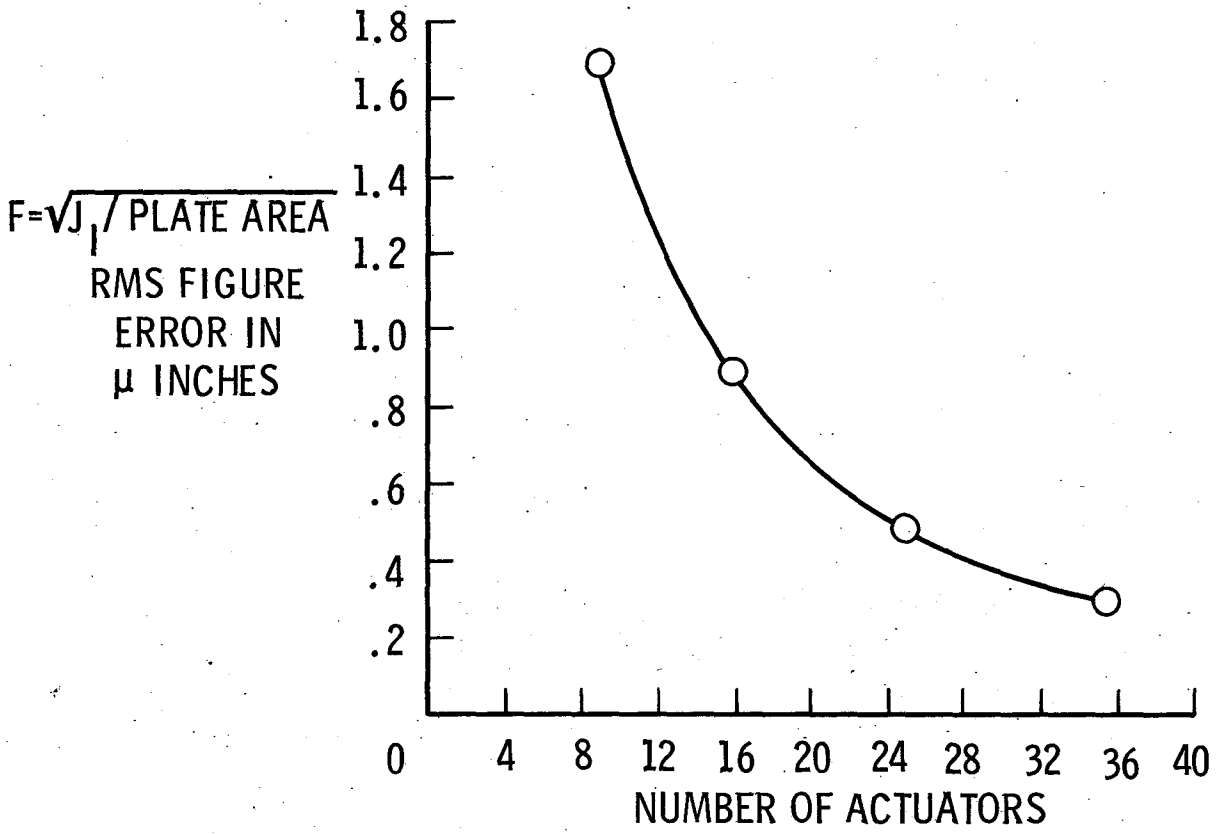

Figure 18.- $\sqrt{J_1/\text{plate area}}$ for a simply supported flat square plate.

The preceding sections contain the development and summary of design considerations for the discrete control of a distributed-parameter system. A simply supported flat rectangular plate has been used as an example because it possesses unique properties which clearly reveal the results of design decisions which are obscured in most distributed system control problems. The following section presents the application of the design technique to a plant which is representative of a thin deformable mirror and whose complexity is more nearly commensurate with that of plants generally encountered in practice.

VII. MODAL CONTROL OF A FREE CIRCULAR PLATE

Modal Representation

The equation of motion of the free circular plate of Fig. 19 under forced vibration is

$$\nabla^2 S \nabla^2 w(r,\theta,t) + \rho \frac{\partial^2 w(r,\theta,t)}{\partial t^2} = p(r,\theta,t) \qquad [68]$$

where w, p, and ∇^2 are expressed in cylindrical coordinates. Assuming solutions separable in r, θ, and t [i.e., $w(r,\theta,t) = c_i(t)f_i(r)v_i(\theta)$], the analysis follows that of the rectangular plate to yield

$$\frac{d^2 c_i(t)}{dt^2} + \omega_i^2 c_i(t) = 0 \qquad [69a]$$

$$\frac{d^2 v_i(\theta)}{d\theta^2} + n^2 v_i(\theta) = 0 \qquad [69b]$$

$$\frac{r^2 d^2[f_i(r)]}{dr^2} + r \frac{df_i(r)}{dr} + (\pm k_i^2 r^2 - n^2) f_i(r) = 0 \qquad [69c]$$

where

$$\omega_i^2 = \frac{S}{\rho} k_i^4 . \qquad [70]$$

Since the mode shape given by [69b] is periodic in θ, n is an integer and

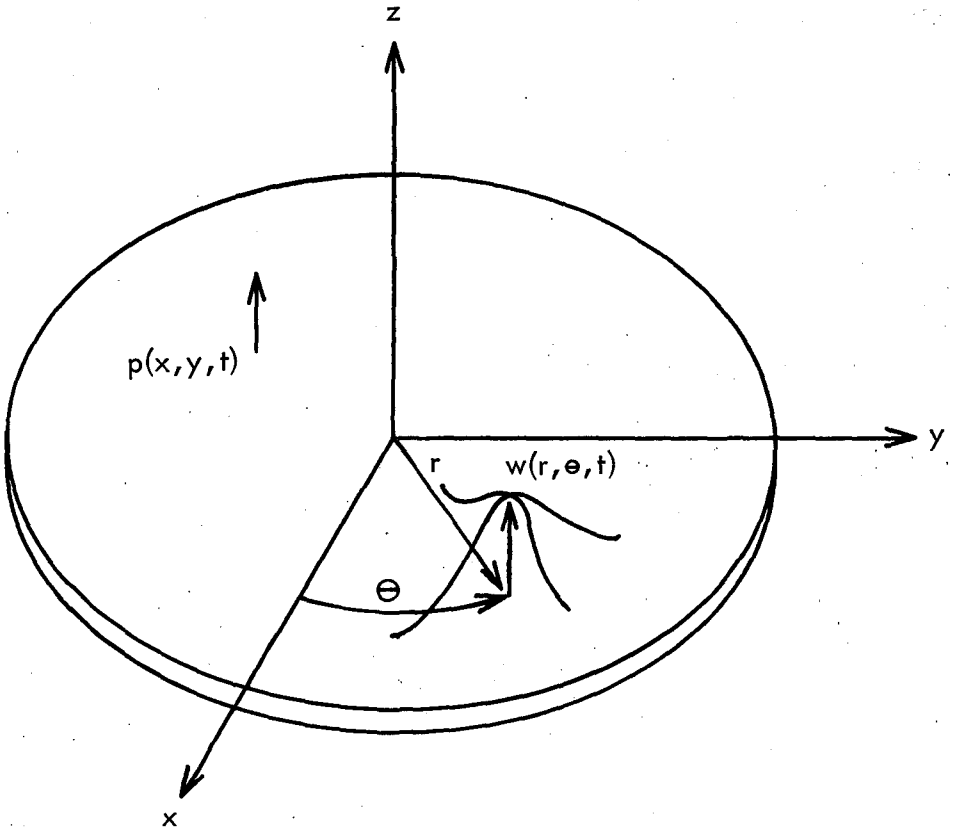

Figure 19.- Free circular plate.

$$u_i(r,\theta) = A\left[J_n(k_i r) + B_i I_n(k_i r)\right]\cos(n\theta + \theta_n) \qquad [71]$$

where A and θ_n are arbitrary constants, J_n and I_n are the n^{th} order Bessel and modified Bessel functions, respectively. The values of k_i and B_i are determined through substitution of [71] into the boundary conditions, which for the free plate, arise from the absence at the free edge of both the bending moment in the radial direction and vertical shear;[10] i.e.,

$$\left(\frac{d^2}{dr^2} + \frac{\nu}{r}\frac{d}{dr} - \frac{n^2\nu}{r^2}\right)f_i(r)\Bigg|_{\text{free edge}} = 0 \qquad [72a]$$

and

$$\left(\frac{d}{dr}\left(\frac{d^2}{dr^2} + \frac{1}{r}\frac{d}{dr} - \frac{n^2}{r^2}\right)f_i(r) + \frac{n^2(\nu - 1)}{r}\frac{d}{dr}\left(\frac{f_i(r)}{r}\right)\right)\Bigg|_{\text{free edge}} = 0. \qquad [72b]$$

Under these conditions there exists a denumerably infinite sequence of eigenvalues

$$k_i = k_{mn} \qquad [73]$$

for which the associated eigenfunctions form a complete orthogonal set permitting both $p(r,\theta,t)$ and $w(r,\theta,t)$ to be expanded in a uniformly convergent series as assumed in Eqs. [12a] and [12b].

Table 2 contains values of k_{mn} for several modes. Because of the importance of the mode shapes relative to design decisions, the radial

m \ n	0	1	2	3	4	5	6	7	8	9
0	0.0	0.0	0.158	0.241	0.318	0.393	0.467	0.540	0.611	0.683
1	.197	.301	.396	.487	.574	.659	.742	.823	.904	.982
2	.412	.515	.612	.706	.796	.884	.973	1.057	1.141	1.225
3	.623	.762	.825	.921	1.014	1.105	1.195	1.283	1.369	1.455
4	.834	.937	1.036	1.134	1.228	1.321	1.413	1.503	1.591	1.680
5	1.045	1.148	1.249	1.346	1.442	1.535	1.628	1.722	1.810	1.900
6	1.254	1.357	1.458	1.557	1.655	1.750	1.843	1.937	2.028	2.117
7	1.463	1.568	1.669	1.769	1.866	1.962	2.055	2.152	2.243	2.335
8	1.675	1.776	1.878	1.977	2.078	2.174	2.270	2.363	2.458	2.55
9	1.883	1.988	2.089	2.189	2.286	2.385	2.482	2.578	2.670	2.765

Table 2.- Values of k_{mn} in inches^{-2} for a free circular plate.

components of the first 21 modes, ranked in order of increasing frequency, ω_i, are plotted in Fig. 20. As a result of the nature of the θ variation in Eq. [71], each pair m,n is associated with two distinct modes given by

$$\text{mode pair m,n} = \begin{cases} f_{mn}(r) \cos n\theta \\ f_{mn}(r) \sin n\theta \end{cases} \qquad [74]$$

for $n \neq 0$. For $n = 0$ a single distinct mode exists for each pair of m,n. To minimize the expectation of the square surface error, the actuators should affect control on the most significant modes as determined by the transmission factor $1/\rho\omega_i^2$ and the disturbance profile. For the purposes of this paper, and as in the case of the rectangular plate, a force distribution with $\sigma_{a_i}^2 = \sigma_{a_j}^2$ is assumed such that an uncontrolled rms figure error of 50×10^{-6} inches (1.27×10^{-4} cm) results. With this white modal disturbance the system objective is to exert control on those modes with the smaller values of k_{mn} in Table 2.

Actuator Size and Placement

The actuators are again modeled as displacement actuators in series with a spring which is attached to the plate by means of a pad. The springs are relatively soft to make the effects of mirror displacement feedback negligible as discussed in Appendix D. The pad shape is a portion of an annulus bounded by constant increments in radius and angle. The elements h_{ij} are evaluated as

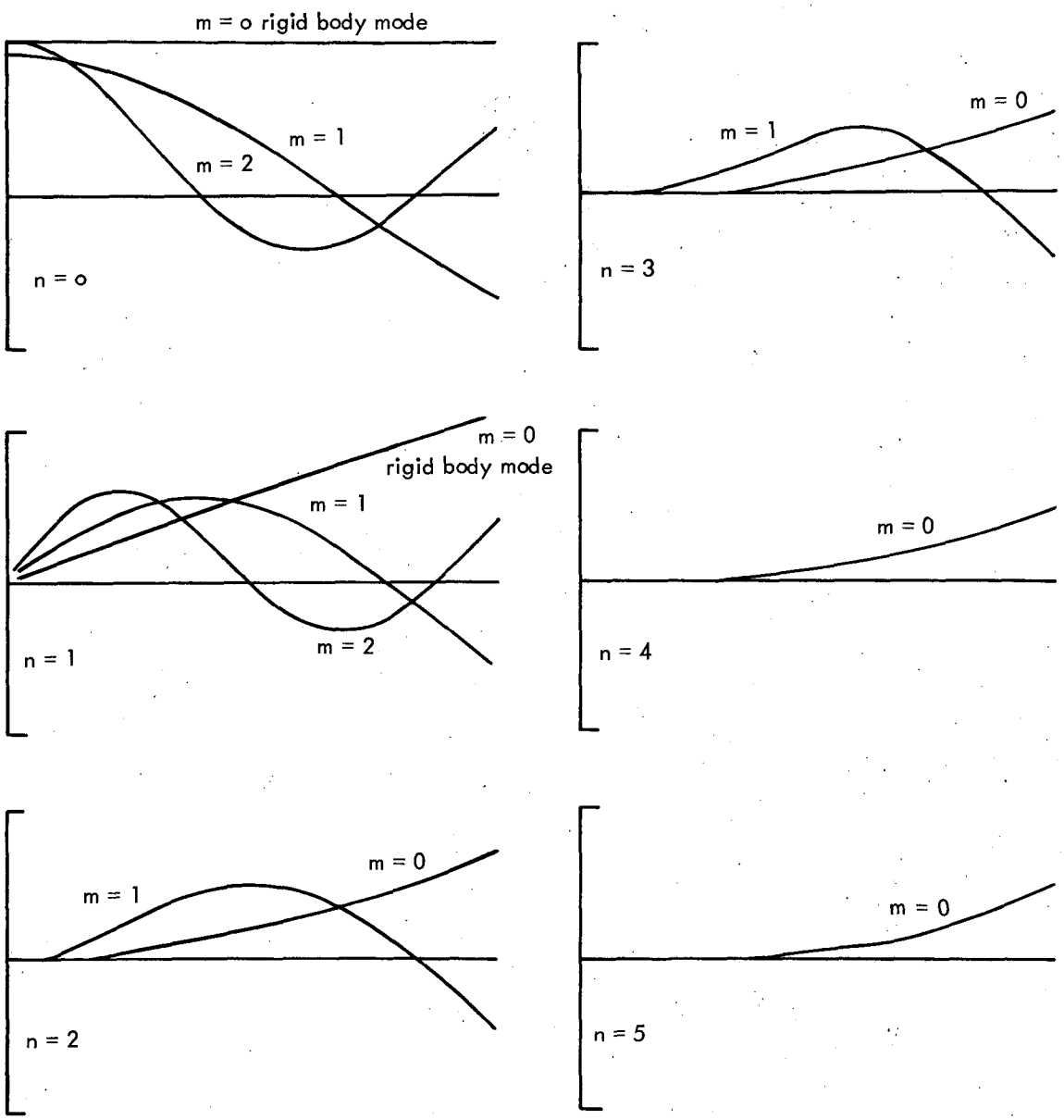

Figure 20.- Modes of free vibration of a free circular plate.

$$\frac{h_{ij}}{\substack{j^{th}\ pad\\ area}} = \frac{1}{\substack{j^{th}\ pad\\ area}} \int_{r_j - \frac{\Delta r_j}{2}}^{r_j + \frac{\Delta r_j}{2}} \int_{\theta_j - \frac{\Delta\theta_j}{2}}^{\theta_j + \frac{\Delta\theta_j}{2}} A\left[J_n(k_{mn}r) + B_i I_n(k_{mn}r)\right] \cos(n\theta + \theta_n) r \, dr \, d\theta \qquad [75]$$

for which the θ dependent component is

$$\Delta\theta_j \frac{\sin(n\Delta\theta_j/2)}{(n\Delta\theta_j/2)} \cos(n\theta_j + \theta_n)$$

where normally the increment $\Delta\theta$ is constant over all j permitting the inclusion of this component in the decoupled plant dynamics. The r component is somewhat less tractable. Under the substitution

$$\eta = k_{mn}r \qquad [76]$$

the r dependent portion of h_{ij} becomes

$$\frac{1}{k_{mn}^2} \int_{k_{mn}\left(r_j - \frac{\Delta r_j}{2}\right)}^{k_{mn}\left(r_j + \frac{\Delta r_j}{2}\right)} A\left[J_n(\eta) + BI_n(\eta)\right] \eta \, d\eta$$

which is integrable if n is an even integer, but requires numerical integration or use of tables if n is odd. The effect in either case is that the radial component of h_{ij} decreases as k_{mn} increases.

In determining the placement of the actuators note from Fig. 20 that each mode m,n has nodes at m distinct locations along lines of constant θ and 2n nodes circularly. The placing of 2n actuators circularly at equal intervals results in their position coinciding with the nodes of one of the modes described by Eq. [74]. Consequently, this mode is not excited while the one spatially shifted 90° is.

To determine the desired actuator placement a knowledge of the disturbance profile is required. Under the earlier assumption of a white modal disturbance spectrum ($\sigma_{a_i}^2 = \sigma_{a_j}^2$), the objective is to control the modes with the smallest values of k_{mn}. Inspection of Table 2 indicates that lines of constant k_{mn} tend to form triangles connecting m to n where

$$n \cong 2m \, . \qquad [77]$$

If the controlled modes are $n \leq n_{max}$ and $m \leq m_{max}$ the controlled area of m,n plane is a rectangle (see Fig. 21a) which should approximate the region of the first N significant nodes. Actuator placement would fall at the nodes of the next highest modes which require

$$N_{actuator} = 2(n_{max} + 1)(m_{max} + 1) \qquad [78]$$

actuators corresponding to the mutual $(m_{max} + 1)$ nodes radially and $2(n_{max} + 1)$ circularly. The controlled modes are the $(2n_{max} + 1)$ $(m_{max} + 1)$ bounded by the rectangle m_{max}, n_{max} plus the $m_{max} + 1$ excited modes for which $n = n_{max} + 1$. Thus, the total number of controlled modes is $N = 2(n_{max} + 1)\,(m_{max} + 1) = N_{actuator}$. The modes

not excited by this actuator placement are those at $n = n_{max} + 1$ whose nodes fall on the lines of constant θ where the actuators are placed (those at $n = n_{max} + 1$ spatially shifted 90° are the extra $m_{max} + 1$ modes included in the N controlled modes). Additionally, the mode whose radial nodes are selected as actuator locations is not excited. The pertinent controlled and unexcited regions of the m,n plane are illustrated in Fig. 21a along with the corresponding actuator placement in Fig. 21b. However, because of the tendency of the lines of constant k_{mn} to form triangles as indicated in Eq. [77], control of an area in the m,n plane as indicated in Fig. 21c is generally desired. This can be accomplished by the actuator placement shown in Fig. 21d. Note that in the latter control scheme while the N most significant modes are controlled, it is not possible to preclude the excitation of the next most significant modes. The trade-off must be made on the basis of actuator location effect on the imaging index J_I.

While, at the present time, the imaging index has been detailed only for the rectangular control scheme illustrated in Fig. 21a, preliminary results indicate that control of the N most significant modes (e.g., see Fig. 21c) is preferred. The rms figuring error $F = \sqrt{J_I/\text{plate area}}$ based on the rectangular control scheme of Fig. 21a is plotted in Fig. 22 versus number of actuators for a plate with the following data:

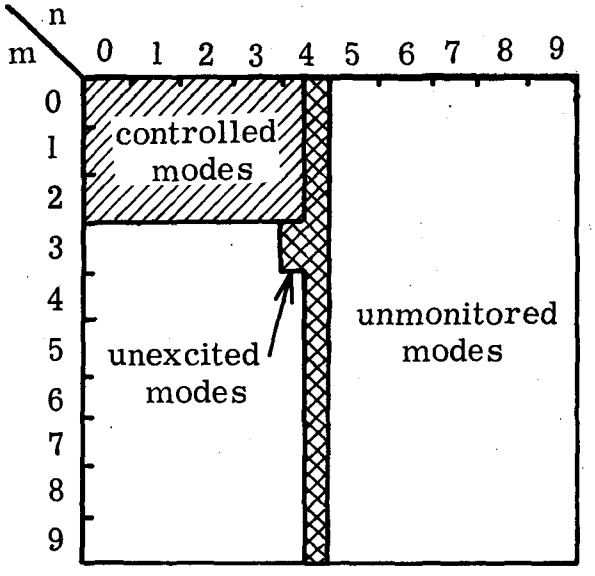

(a) The m,n plane for the actuator placement of b.

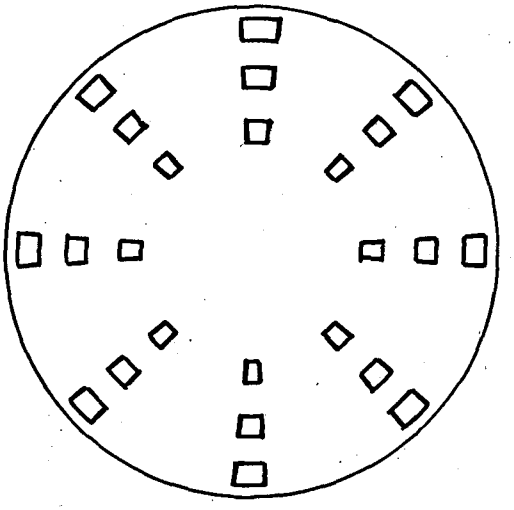

(b) An actuator configuration utilizing twenty-four actuators.

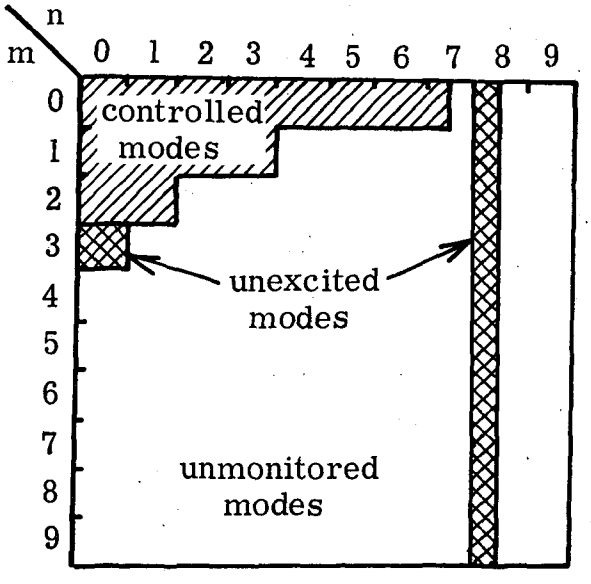

(c) The m,n plane for the actuator placement of d.

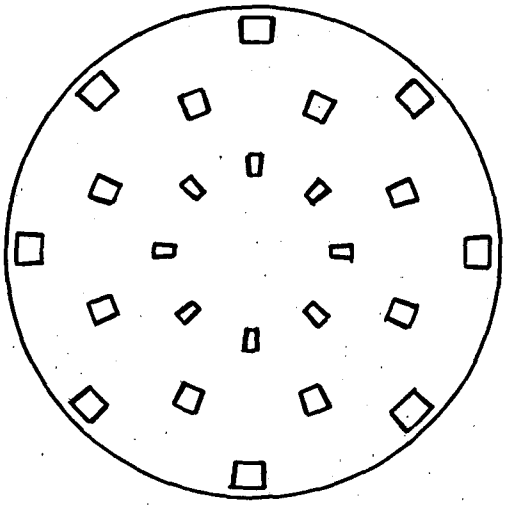

(d) An alternate actuator configuration utilizing twenty-four actuators.

Figure 21.- The location in the m,n plane of the controlled, unexcited, and unmonitored modes of a free circular plate.

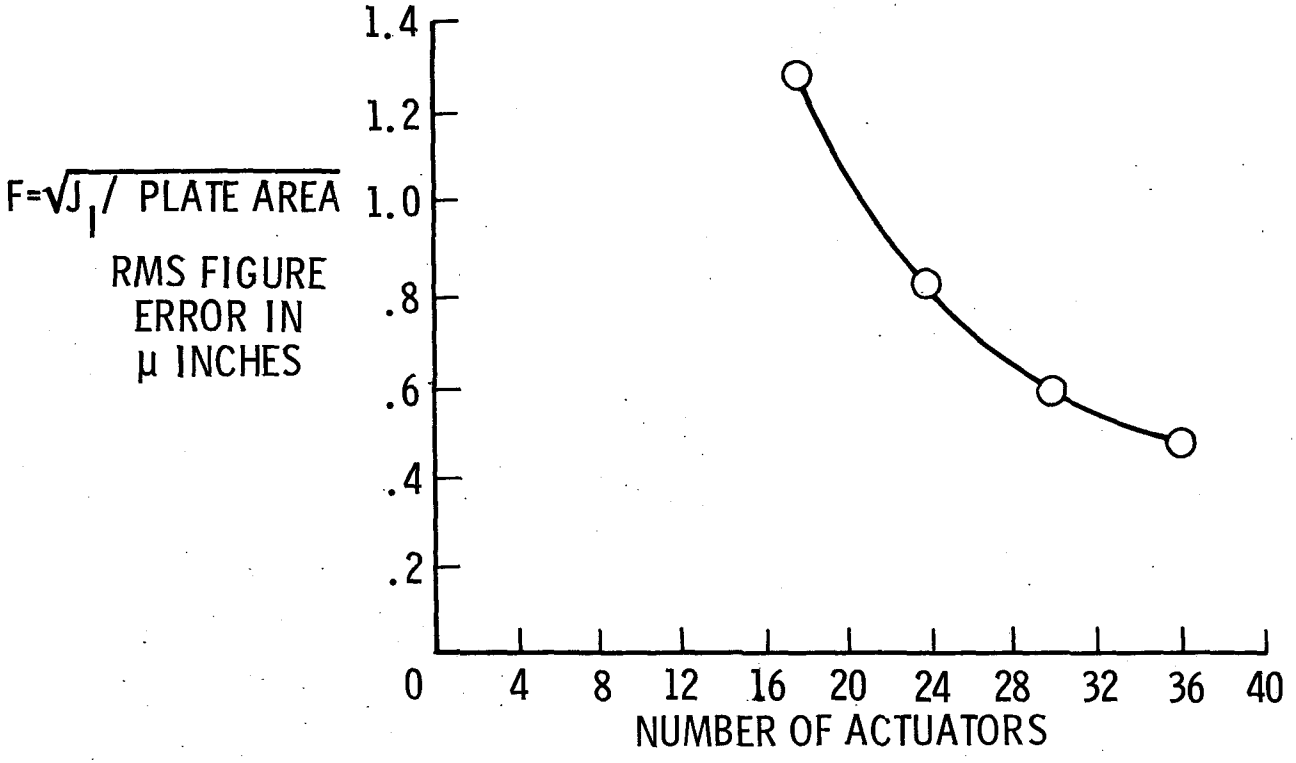

Figure 22.- $\sqrt{J_1/\text{plate area}}$ for a flat circular free plate.

Thickness	0.5 inch (1.27 cm)
Diameter	30 inches (76.2 cm)
Young's modulus	10^7 psi (70.3×10^7 gm/cm^2)
Poisson's ratio	0.2

These results indicate satisfactory control, yielding diffraction-limited performance, as defined by an rms figure error of less than 0.5μ inches, is achieved with less than 24 actuators. This is significantly less than the 61 actuators used in the present laboratory model[14] which was determined by sectioning the mirror into equilateral triangles 3.75 inches on a side (the 3.75" × 3.75" × 3.75" × 0.5" thick triangles represent a thickness-to-area ratio near that normally found in monolithic telescope mirrors).

VIII. CONCLUDING REMARKS

The modal expansion technique has been applied to the problem of correcting and maintaining, to the tolerance required for diffraction-limited performance, the optical figure of a plant representative of the primary mirror of an orbiting astronomical observatory. The modal technique has been shown to be particularly appropriate for this problem by virtue of its relevance to a useful measure of image quality, its ability to decouple the system dynamics permitting simple control techniques to be applied, and by the extent of the insight the technique affords into engineering design decisions.

For distributed plants subject to extremely accurate control, it is necessary to consider the effects on system performance of all of the modes - not just those which are subject to control. In fact, with the error in the modes under control reduced to any desired level, the major system error was shown to reside in the uncontrolled higher-order modes and this is increased by the control effort applied to the lower modes. For this reason the most significant design decisions are those related to the effects of the corrective control forces on the higher-order modes. The analysis presented in this paper describes the effect of actuator size and location on system performance, factors most critical to efficient design. The requisite conditions for minimizing the number of discrete control inputs required to achieve satisfactory performance were outlined and then illustrated in two design examples. The results for both the rectangular plate and the

free circular plate indicate that the thin deformable mirror can provide diffraction-limited performance; further, that this performance can be achieved with considerably less actuators than that required for a segmented mirror where the thickness-to-area ratio for each segment approaches that normally used in monolithic mirrors.

The disturbance profile (if data on the effects of thermal gradients, spontaneous release of material stresses, or other factors producing distortion of the optical surface become available) can be readily incorporated into the design procedure. This is achieved by using the profile along with the transmission properties of the plant (plate) to determine the modal errors and the N modes yielding the largest errors controlled. Extension to more complex plants (e.g., shells), while requiring considerable computing effort, is direct.

REFERENCES

(1) Gould, L. A., and Murray-Lasso, M. A., "On the Modal Control of Distributed Systems With Distributed Feedback," IEEE Trans. on Automatic Control, Vol. AC-11, No. 4, October 1966, pp. 729-736.

(2) Lindgren, A. G., "A Note on Stability and Design of Interacting Multivariable Control Systems," IEEE Trans. on Automatic Control, Vol. AC-11, No. 2, April 1966, pp. 314-315.

(3) Goody, R. M., Atmospheric Radiation-I Theoretical Basis, Oxford Monographs on Meteorology, Oxford University Press, Amen House, London, England, 1964.

(4) Fredrick, L. W., ed., "Applications in Astronomy Suitable for Study by Means of Manned Orbiting Observatories and Related Instrumentation and Operational Requirements," NASA CR-52897 (Vol. 1) and NASA CR-52902 (Vol. 2) Leander McCormick Observatory, University of Virginia, Charlottesville, Va., 1963.

(5) Howell, W. E., "Technology for a Manned Orbiting Telescope," Proc. of the Space Optical Technology Conference, Vol. 1, NASA-Langley Research Center, Langley Station, Hampton, Va., April 1966.

(6) Robertson, H. J., et al., "Active Optical System for Spaceborne Telescopes," NASA CR-66297, Perkin-Elmer Co., Norwalk, Connecticut, October 14, 1966.

(7) Robertson, H. J., et al., "Active Optical System for Spaceborne Telescopes," Vol. II, NASA CR-66489, Perkin-Elmer Co., Norwalk, Connecticut, December 7, 1967.

(8) Robertson, H. J., "Development of an Active Optics Concept Using a Thin Deformable Mirror," NASA CR-1593, Perkin-Elmer Co., Norwalk, Connecticut, 1970.

(9) Greensite, A. L., "Analyses and Design of Space Vehicle Flight Control Systems," Vol. XII - Attitude Control in Space. NASA CR-831, General Dynamics Corp., San Diego, Calif., August 1967.

(10) Timoshenko, S., and Woinowsky-Kreiger, S., Theory of Plates and Shells, Second Edition, McGraw-Hill Book Company, New York, N.Y., 1959.

(11) Courant, R., and Hilbert, D., Methods of Mathematical Physics, First English Edition, Interscience Publishers, Inc., New York, N.Y., 1937.

(12) Born, M., and Wolf, E., Principles of Optics, Second Edition, MacMillan Company, New York, N.Y., 1964.

(13) Truxal, J. G., "Control Systems - Some Unusual Design Problems," Chapter 4, Adaptive Control Systems, Mishken, E., and Braun, L., (eds.), McGraw-Hill Book Company, Inc., New York, N.Y., 1961.

(14) Creedon, J. F., and Robertson, H. J., "Evaluation of Multipoint Interaction in the Design of a Thin Diffraction-Limited Active Mirror," IEEE Trans. on Aerospace and Electronics Systems, Vol. AES-5, No. 2, March 1969, pp. 287-293.

(15) Wylie, C. R., Jr., Advanced Engineering Mathematics, Third Edition, McGraw-Hill Book Company, New York, N.Y., 1966.

APPENDIX A

Determination of the Eigenfunctions and Eigenvalues of a Simply Supported Flat Rectangular Plate

The equation of motion of a uniform plate in forced vibration[9] is

$$\nabla^2 S \nabla^2 w(x,y,t) + \rho \frac{\partial^2 w(x,y,t)}{\partial t^2} = p(x,y,t) \qquad [A1]$$

consider first the homogeneous equation. The modes of free vibration will be determined through the separation of variables technique by assuming

$$w(x,y,t) = w_1(t) w_2(x,y) \qquad [A2]$$

Substituting [A2] into [A1]

$$w_1(t) S \nabla^4 w_2(x,y) + \rho\, w_2(x,y) \frac{\partial^2 w_1(t)}{\partial t^2} = 0 \qquad [A3]$$

dividing both sides by $\rho_o w_1(t) w_2(x,y)$ yields

$$\frac{S}{\rho} \frac{\nabla^4 w_2(x,y)}{w_2(x,y)} = - \frac{1}{w_1(t)} \frac{\partial_1^2 w_1(t)}{\partial t^2} \qquad [A4]$$

Since each side of [A4] is a function of different variables, both sides are set equal to ω_i^2 - a positive constant. This yields the following equations

$$\frac{S}{\rho} \nabla^4 w_2(x,y) - \omega_i^2 w_2(x,y) = 0 \qquad [A5]$$

$$\frac{\partial^2 w_1(t)}{\partial t^2} + \omega_i^2 w_1(t) = \frac{dw_1(t)}{dt^2} + \omega_i^2 w_1(t) = 0 \qquad [A6]$$

Rearranging [A5] yields

$$\nabla^4 w_2(x,y) - \frac{\omega_i^2 \rho\, w_2(x,y)}{S} = 0 \qquad [A7]$$

or

$$\left(\nabla^2 + \omega_i\sqrt{\frac{\rho}{S}}\right)\left(\nabla^2 - \omega_i\sqrt{\frac{\rho}{S}}\right) w_2(x,y) = 0 \qquad [A8]$$

The solution to [A8] is the sum of the solutions to each of the products of [A8] or therefore to

$$\left(\nabla^2 + \omega_i\sqrt{\frac{\rho}{S}}\right) w_2(x,y) = 0 \qquad [A9]$$

$$\left(\nabla^2 - \omega_i\sqrt{\frac{\rho}{S}}\right) w_2(x,y) = 0 \qquad [A10]$$

∇^2 is the Laplacian in Cartesian coordinates. Equations [A9] and [A10] are therefore

$$\frac{\partial^2}{\partial x^2} w_2(x,y) + \frac{\partial^2}{\partial y^2} w_2(x,y) \pm \omega_i\sqrt{\frac{\rho}{S}}\, w_2(x,y) = 0 \qquad [A11]$$

A further assumption is made that

$$w_2(x,y) = w_3(x)w_4(y) \qquad [A12]$$

In this case [A11] becomes

$$w_4(y)\frac{d^2w_3(x)}{dx^2} + w_3(x)\frac{d^2w_4(y)}{dy^2} \pm \omega_i\sqrt{\frac{\rho}{S}}\, w_3(x)w_4(y) = 0 \qquad [A13]$$

Dividing by $w_3(x)w_4(y)$ and rearranging yields first

$$\frac{1}{w_3(x)}\frac{d^2w_3(x)}{dx^2} + \frac{1}{w_4(y)}\frac{d^2w_4(y)}{dy^2} \pm \omega_i\sqrt{\frac{\rho}{S}} = 0 \qquad [A14]$$

then

$$\frac{1}{w_3(x)}\frac{d^2w_3(x)}{dx^2} \pm \omega_i\sqrt{\frac{\rho}{S}} = -\frac{1}{w_4(y)}\frac{d^2w_4(y)}{dy^2} \qquad [A15]$$

Since the left side is equal to a function of x, and the right a function of y both sides must be equal to a constant $+\mu^2$. (The choice of sign on μ^2 is arbitrary since choosing as the constant $-\mu^2$ will yield the same answers.) Equation [A15] becomes

$$\frac{d^2w_3(x)}{dx^2} + \left(-\mu^2 \pm \omega_i\sqrt{\frac{\rho}{S}}\right)w_3(x) = 0 \qquad [A16]$$

and

$$\frac{d^2w_4(y)}{dy^2} + \mu^2 w_4(y) = 0 \qquad [A17]$$

The solutions to these equations are

$$w_3(x) = A_1 \sin\left(\sqrt{-\mu^2 \pm \omega_i\sqrt{\frac{\rho}{S}}}\, x + \xi_1\right) \qquad [A18]$$

and

$$w_4(y) = A_2 \sin(\mu y + \xi_2), \qquad [A19]$$

respectively.

From equations [A12], [A18], and [A19] the solution to equation [A5] is

$$w_2(x,y) = A_3 \sin\left(\sqrt{-\mu^2 \pm \omega_i\sqrt{\frac{\rho}{S}}}\, x + \xi_1\right) \sin(\mu y + \xi_2) \qquad [A20]$$

where A_3 is the product of A_1 and A_2. In order to evaluate the constants in [A20] the boundary conditions must be specified. For a simply supported flat plate they are[10]

$$w_2(x,y) = 0 \quad \text{for} \quad \begin{matrix} x = 0,a \\ y = 0,b \end{matrix} \qquad [A21]$$

$$M_x = 0 = -S\left(\frac{\partial^2 w_2(x,y)}{\partial x^2} + \nu \frac{\partial^2 w_2(x,y)}{\partial y^2}\right)\Bigg|_{\substack{x=0 \\ x=a}} \qquad [A22]$$

and

$$M_y = 0 = -S\left(\frac{\partial^2 w_2(x,y)}{\partial y^2} + \nu \frac{\partial^2 w_2(x,y)}{\partial x^2}\right)\Bigg|_{\substack{y=0\\y=b}} \qquad [A23]$$

In light of [A21] the equations [A22] and [A23] may be written as

$$\frac{\partial^2 w_2(x,y)}{\partial x^2}\Bigg|_{\substack{x=0\\x=a}} = 0 \qquad [A24]$$

and

$$\frac{\partial^2 w_2(x,y)}{\partial y^2}\Bigg|_{\substack{y=0\\y=b}} = 0 \qquad [A25]$$

Using the conditions for $x = 0$, $y = 0$ from equation [A21] in [A20] yields

$$\xi_1 = \xi_2 = 0 \qquad [A26]$$

Using the condition of equation [A21] for $y = b$ yields

$$\sin \mu b = 0 \qquad [A27]$$

and therefore

$$\mu = \frac{n\pi}{b} \qquad n = 0, 1, 2, \ldots \qquad [A28]$$

From the condition for x = a

$$\sin\left(-\mu^2 \pm \omega_i\sqrt{\frac{\rho}{S}}\right)a = 0 \qquad [A29]$$

or

$$\left(-\mu^2 \pm \omega_i\sqrt{\frac{\rho}{S}}\right) = \frac{m\pi}{a} \qquad m = 0, 1, 2 \qquad [A30]$$

Substituting [A28] and [A30] into [A20] gives in [A31] the shape of the modes of free vibration, or eigenfunctions, of the plate

$$w_2(x,y) = A_3 \sin\frac{m\pi x}{a}\sin\frac{n\pi y}{b} \qquad n,m = 1, 2, 3, \ldots \qquad [A31]$$

The resulting mode shape is identically zero for either m or n zero, consequently, equation [A31] is valid for the range of m and n indicated.

That equation [A31] satisfies [A24] and [A25] may be verified through substitution. Further, A_3 may be chosen to satisfy the requirement

$$\int_0^b \int_0^a \omega_i^2(x,y)\,dx\,dy = 1 \qquad [A32]$$

which yields

$$A_3 = \frac{4}{ab} \qquad [A33]$$

$$w_2(x,y) = \frac{4}{ab} \sin \frac{m\pi x}{a} \sin \frac{n\pi y}{b} \qquad [A34]$$

Since from [A4] $\omega_i^2 = \frac{S}{\rho} \frac{\nabla^4 w_2(x,y)}{w_2(x,y)}$

$$\omega_i^2 = \frac{\frac{S}{\rho}\left[\frac{\partial^4}{\partial x^4} + \frac{\partial^2}{\partial x^2}\frac{\partial^2}{\partial y^2} + \frac{\partial^4}{\partial y^2}\right] w_2(x,y)}{w_2(x,y)} \qquad [A35]$$

$$\omega_i^2 = \frac{S}{\rho} \frac{1}{w_2(x,y)}\left[\frac{m^4\pi^4}{a^4} w_2(x,y) + \frac{m^2\pi^2}{a^2}\frac{n^2\pi^2}{b^2} w_2(x,y) + \frac{n^4\pi^4}{b^4} w_2(x,y)\right] \qquad [A36]$$

$$\omega_i^2 = \frac{S\pi^4}{\rho}\left[\frac{m^2}{a^2} + \frac{n^2}{b^2}\right]^2 = \omega_{mn}^2 \qquad [A37]$$

This could also have been obtained from [A27], [A28], and [A30].

Since the solution to (6) is

$$w_1(t) = A_4 \cos\left(\omega_i t + \xi_i\right) \qquad [A38]$$

The most general solution to the homogeneous form of [A1] is

$$w(x,y,t) = \sum_{m,n=1}^{\infty} A_{mn} \cos(\omega_{mn} + \xi_{mn}) \sin \frac{n\pi x}{a} \sin \frac{m\pi y}{b} \qquad [A39]$$

Thus the eigenfunctions or modes of free vibration and their associated eigenvalues have been determined for a simply supported, flat, rectangular plate and are given by equations [A34] and [A37] respectively.

APPENDIX B

Determination of a Set of Actuator Locations for Which U^N For a Simply Supported Flat Rectangular Plate is Orthogonal

The purpose of this appendix is to indicate, for a simply supported, flat, rectangular plate a set of actuator locations which make the U^N matrix (eq. [34]) orthogonal. The equation of motion of a beam[15] is

$$\tau^2 \frac{\partial^4 w(x,t)}{\partial x^4} = - \frac{\partial^2 w(x,t)}{dt^2} \qquad [B1]$$

The method of separation of variables is used, consequently,

$$w(x,t) = w_1(x) w_2(t) \qquad [B2]$$

Substituting [B2] into [B1] gives, after dividing both sides by $w(x,t)$,

$$\frac{\tau^2}{w_1(x)} \frac{d^4 w_2(x)}{dx^4} = \frac{1}{w_2(t)} \frac{d^2 w_2(t)}{dt^2} \qquad [B3]$$

Both sides are set equal to a constant γ^4

$$\tau^2 \frac{d^4 w_1(x)}{dx^4} - \gamma^4 w_1(x) = 0 \qquad [B4a]$$

$$\frac{d^2 w_2(t)}{dt^2} + \gamma^4 w_2(t) = 0 \qquad [B4b]$$

The solution to [B4b] is

$$w_2(t) = C_1 \sin \gamma^2 t + C_2 \cos \gamma^2 t \qquad [B5]$$

The solution to the remaining equation, [B4a], will yield the modes of free vibration of the beam. Since the exact solution will be used in the sequel this information will be obtained first.

Equation [B4a] is factored as

$$\left(\frac{d^2}{dx^2} - \frac{\gamma^2}{\tau}\right)\left(\frac{d^2}{dx^2} + \frac{\gamma^2}{\tau}\right)w_1(x) = 0 \qquad [B6]$$

and the solution is the sum of the solutions to

$$\left(\frac{d^2}{dx^2} - \frac{\gamma^2}{\tau}\right)w_1(x) = 0 \qquad [B7]$$

and

$$\left(\frac{d}{dx^2} + \frac{\gamma^2}{\tau}\right)w_1(x) = 0 \qquad [B8]$$

Thus

$$w_1(x) = C_3 \cos \frac{\gamma}{\sqrt{\tau}} x + C_4 \sin \frac{\gamma}{\sqrt{\tau}} + C_5 \cosh \frac{\gamma}{\sqrt{\tau}} + C_6 \sinh \frac{\gamma}{\sqrt{\tau}} \qquad [B9]$$

at this point the boundary conditions are brought in. For a simply supported beam (10)

$$w_1(0) = 0 \qquad [B10a]$$

$$w_1(b) = 0 \qquad [B10b]$$

and there are no moments at either x = 0 or x = b

$$\left.\frac{d^2 w_1(x)}{dx^2}\right|_{\substack{x=0 \\ x=b}} = 0 \qquad [B10c]$$

These conditions require

$$0 = C_3 + C_5 \qquad [B11a]$$

$$0 = C_3 \cos \frac{\gamma}{\sqrt{\tau}} b + C_4 \sin \frac{\gamma}{\sqrt{\tau}} b + C_5 \cosh \frac{\gamma}{\sqrt{\tau}} b + C_6 \sinh \frac{\gamma}{\sqrt{\tau}} b \qquad [B11b]$$

$$0 = -\frac{\gamma^2}{\tau} C_3 + \frac{\gamma^2}{\tau} C_5 \qquad [B11c]$$

$$0 = -\frac{\gamma^2}{\sqrt{\tau}}\left[C_3 \cos \frac{\gamma}{\sqrt{\tau}} b + C_4 \sin \frac{\gamma}{\sqrt{\tau}} b\right] + \frac{\gamma^2}{\sqrt{\tau}}\left[C_5 \cosh \frac{\gamma}{\sqrt{\tau}} b + C_6 \sinh \frac{\gamma}{\sqrt{\tau}} b\right] \qquad [B11d]$$

From equations [B11a] and [B11c] it is determined that

$$C_3 = C_5 = 0 \qquad [B12]$$

leaving

$$0 = C_4 \sin \frac{\gamma b}{\sqrt{\tau}} + C_6 \sinh \frac{\gamma}{\sqrt{\tau}} b \qquad [B13]$$

$$0 = -C_4 \sin \frac{\gamma b}{\sqrt{\tau}} + C_6 \sinh \frac{\gamma}{\sqrt{\tau}} b \qquad [B14]$$

A nontrivial result requires the determinant of the coefficients of C_4 and C_6 in equations [B13] and [B14] to be zero. Consequently,

$$2 \sin \frac{\gamma b}{\sqrt{\tau}} \sinh \frac{\gamma b}{\sqrt{\tau}} = 0 \qquad [B15]$$

or

$$\frac{\gamma b}{\sqrt{\tau}} = m\pi \qquad [B16]$$

Substitution of [B16] into [B13] indicates that $C_6 = 0$ and

$$\frac{\gamma}{\sqrt{\tau}} = \frac{m\pi}{b} \qquad [B17]$$

The eigenfunction of the homogeneous simply supported beam is

$$w_1(x) = C_4 \sin \frac{m\pi}{b} x \qquad [B18]$$

The solution to the problem is now considered through the method of finite differences. A number of stations are located at equal intervals, l, along the beam as shown in the following sketch

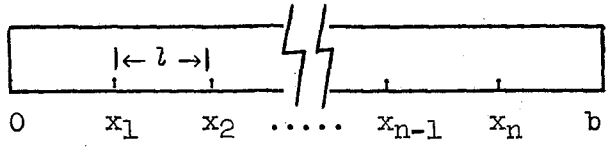

and the equation

$$\frac{d^4 w^N}{dx^4} - \frac{\gamma^4}{\tau^2} w^N = 0 \qquad [B19]$$

is written at each point, where $w^N = \text{col } \omega(x_1), \ldots \omega(x_n)$. The fourth derivative approximation used can be obtained by first obtaining the

Taylor series expansions about x_r of $w(x_{r+1})$, $w(x_{r+2})$, $w(x_{r-1})$, $w(x_{r-2})$. These expressions are

$$w(x_{r+1}) = w(x_r) + w'(x_r)l + w''(x_r)\frac{l^2}{2!} + \ldots + w^{(n)}(x_r)\frac{l^n}{n!} \quad [B20a]$$

$$w(x_{r-1}) = w(x_r) - w'(x_r)l + w''(x_r)\frac{l^2}{2!} - \ldots + (-1)^n w^{(n)}(x_r)\frac{l^n}{n!} \quad [B20b]$$

$$w(x_{r+2}) = w(x_r) + w'(x_r)2l + w''(x_r)\frac{(2l)^2}{2!} + \ldots + w^{(n)}(x_r)\frac{(2l)^n}{n!} \quad [B20c]$$

$$w(x_{r-2}) = w(x_r) - w'(x_r)2l + w''(x_r)\frac{(2l)^2}{2!} + \ldots + (-1)^n w^{(n)}(x_r)\frac{(2l)^n}{n!} \quad [B20d]$$

subtracting four times ([B20a] + [B20b]) from [B20c] + [B20d] yields

$$-4\left[w(x_{r+1}) + w(x_{r-1})\right] + w(x_{r+2}) = -6w(x_r) + 2\left.\frac{d^4w(x)}{dx^4}\right|_{x=x_r}\frac{l^4}{4!}(2^4 - 4) + \ldots + 2\left.\frac{d^{2m}w(x)}{dx^{2m}}\right|_{x=x_r}\frac{l^{2m}}{(2m)!}(2^{2m} - 4) + \ldots \quad [B21]$$

After rearranging equation [B21] becomes

$$\frac{w(x_{r-2}) - 4w(x_{r-1}) + 6w(x_r) - 4w(x_{r+1}) + w(x_{r+2})}{l^4} = \left.\frac{d^4w(x)}{dx^4}\right|_{x=x_r} + \cdots + 2\left.\frac{d^{2m}w(x)}{dx^{2m}}\right|_{x=x_r} \frac{l^{2(m-2)}2^{2(m-1)}}{(2m)!} + \cdots \qquad [B22]$$

The term on the left will be denoted L_{fd}. The finite difference method approximates the plant equation as

$$L_{fd}w(x_r) - \frac{\gamma_{fd}^4}{\tau^2} w(x_r) = 0 \qquad [B23]$$

Collecting the expressions for each point and arranging them as indicated by the definition of w^N yields the matrix equation.

$$L_{fdm}\begin{bmatrix} w(x_1) \\ \vdots \\ w(x_n) \end{bmatrix} = \frac{\gamma_{fd}^2}{\tau}\begin{bmatrix} w(x_1) \\ \vdots \\ w(x_n) \end{bmatrix} \qquad [B24]$$

The solutions to this equation are the eigenvectors of the finite difference - matrix representation of the plant, L_{fdm}. The matrix is a real symmetric matrix and consequently, has orthogonal eigenfunctions.

If the right-hand side of equation [B22] is used instead of the left it is possible to obtain an analytic expression for the numerically

obtained finite difference answers. That is, consider the equation

$$0 = \frac{d^4 w(x)}{dx^4} - \frac{\gamma_{fd}^2}{\tau} w(x) + \ldots + 2 \frac{d^{2m} w(x)}{dx^{2m}} \frac{l^{2(m-2)}}{(2m)!} 2^{2(m-1)} + \ldots \qquad [B25]$$

The answer to this equation evaluated at $x = x_r$ is equal to the finite difference answer.

Consider the function $u_i = C_4 \sin \frac{\gamma}{\sqrt{b}} x$ which, from [B18], is seen to be the exact eigenfunction. Substituting this expression into [B25] yields, after cancelling u_i

$$0 = \frac{\gamma^4}{\tau^2} - \frac{\gamma_{fd}^4}{\tau^2} + \ldots + (-1)^m \left(\frac{\gamma}{\sqrt{\tau}}\right)^{2m} \frac{l^{2(m-2)}}{(2m)!} 2^{2(m-1)} + \ldots \qquad [B26]$$

Thus $u_i(x)$ is the solution to [B25], and $u_i(x_1) = w(x_i)$, when

$$\frac{\gamma_{fd}^4}{\tau^2} = \frac{\gamma^4}{\tau^2} + \ldots + \frac{(-1)^m}{(2m)!} \left(\frac{\gamma}{\sqrt{\tau}}\right)^{2m} \frac{(2l)^{2(m-1)}}{l^2} + \ldots \qquad m \geq 3 \qquad [B27]$$

l is the separation between adjacent stations on the beam and it can be made as small as desired. Consequently, equation [B27] indicates the resultant convergence of $\frac{\gamma_{fd}}{\sqrt{\tau}}$ to $\frac{\gamma}{\sqrt{\tau}}$. More significant for the purpose of this appendix is the fact that the i^{th} component of the j^{th} eigenvector of the finite difference solution is equivalent to the j^{th} eigenfunction of the beam evaluated at a location corresponding

to the i^{th} point in the finite difference representation of the beam. Since the matrix U^N of Eq. [34] is

$$U^N = \begin{bmatrix} u_1(x_1) & \cdots & u_N(x_1) \\ \vdots & \ddots & \vdots \\ u_1(x_N) & \cdots & u_N(x_N) \end{bmatrix} \qquad [B28]$$

each column corresponds to one of the orthogonal eigenvectors of L_{fdm} and the matrix U^N is itself orthogonal.

To this point the proof has concerned the solution for a beam, while it is desired to show

$$\sum_{k=1}^{N} u_i(x_k)u_j(x_k) = 0 \qquad i \neq j \qquad [B29]$$

for the plate. For the plate, Appendix A shows that

$$u_i(x_k) = C_i \sin \frac{m_i \pi x_k}{a} \sin \frac{n_i \pi y_k}{b} \qquad [B30]$$

consequently, Eq. [B29] may be written

$$\sum_{k=1}^{N} u_i(x_k)u_j(x_k) = \sum_{k=1}^{N} u_{xi}(x_k)u_{yi}(y_k)u_{xj}(x_k)u_{yj}(y_k) \qquad [B31]$$

Consider an array of locations

$$N = XY \qquad [B32]$$

with X locations in the x direction and Y in the y direction. Thus [B31] becomes

$$\sum_{k=1}^{N} u_{xi}(x_k)u_{yi}(y_k)u_{xj}(x_k)u_{yj}(x_k) = \sum_{A_3=1}^{X}\sum_{B_4=1}^{Y} u_{xi}(x_A)u_{yi}(y_B)u_{xj}(x_A)u_{yj}(y_B) \qquad [B33]$$

or

$$= \sum_{A_3=1}^{X} u_{xi}(x_A)u_{xj}(x_A) \sum_{B_4=1}^{Y} u_{yi}(x_B)u_{yj}(x_B)$$

Each component in the second expression for the right-hand side of [B33] is equivalent to the beam, consequently, either the first or second summation will be zero unless i = j.

Equally spaced points will provide an orthogonal matrix for the purpose of relating performance specification in the original and transformed systems.

APPENDIX C

Evaluation of the RMS Figuring Error for a Simply Supported Flat Rectangular Plate

The purpose of this appendix is to describe in detail one of the procedures used in determining the results contained in Figure 18. As indicated in equations [42] and [67] the exact determination of J_I would require the evaluation of an infinite number of terms. In using a finite number of terms P to approximate J_I and, therefore the rms error, it is desired to select such a P, if possible, which would place a bound on the amount by which the approximate value of J_I would differ from the true value.

The value of P which should be used is a function of the individual terms in the sequences

$$a_1, a_2, \cdots a_n \cdots \qquad [C1]$$

and

$$\omega_1^2, \omega_2^2, \cdots \omega_n^2 \cdots \qquad [C2]$$

Since

$$c_{i_{ss}} = \frac{a_{i_{ss}}}{\rho\omega_i^2} \qquad [C3]$$

one procedure might be, for monotonically decreasing values of $c_{i_{ss}}$, to observe values of $c_{i_{ss}}$ in [C3] for increasing i until values of $c_{i_{ss}}$ are obtained which are significantly less than the accuracy desired.

The value of J_I may be determined for two values of P in this neighborhood to determine whether or not J_I has been obtained accurately enough.

While such a procedure would be adequate the specific nature of the present problem permits the selection of P on a more rigorous basis. For a square plate the expression contained in Appendix A for the eigenvalues becomes

$$\omega_i^2 = \frac{S\pi^4}{\rho a^4}\left[m_i^2 + n_i^2\right]^2 \qquad [C4]$$

From Eqs. [2], [15], and [C3], and [C4]

$$\int_o^a \int_o^b w^2(x,y,t)dx\,dy = \sum_{i=1}^{\infty} \frac{a_8 a_i^2}{\left[S\pi^4\right]^2\left[m_i^2 + n_i^2\right]^4} \qquad [C5]$$

Since m and n each take on the values of all the positive integers the right-hand side of [C5] may be rewritten

$$\sum_{i=1}^{\infty} \frac{a^8}{\left[S\pi^4\right]^2}\left[m_i^2 + n_i^2\right]^4 = \frac{a^8}{\left[S\pi^4\right]^2}\sum_{i=1}^{\infty}\sum_{j=1}^{\infty} \frac{a_{ij}^2}{\left[i^2 + j^2\right]^4} \qquad [C6]$$

In order to remove one of the infinite summations, use is made of the symmetry of the eigenvalues by writing [C6] as

$$\frac{a^8}{\left[\pi^4 S\right]^2}\sum_{i=1}^{\infty}\sum_{j=1}^{\infty} \frac{a_{ij}^2}{\left[i^2 + j^2\right]^4} < 2\,\frac{a^8 a_{ij}^2}{\left[S\pi^4\right]^2}\sum_{i=1}^{\infty}\sum_{j=1}^{i} \frac{1}{\left[i^2 + j^2\right]^4} \qquad [C7]$$

where a_{ij} is considered a constant as has already been assumed (see Eq. [66]). The terms $i^2 + j^2$ in the series

$$\sum_{i=1}^{\infty} \sum_{j=1}^{i} \frac{1}{\left[i^2 + j^2\right]^4} \qquad [C8]$$

are placed into correspondence with the positive integers in the order indicated by [C8]. It is desired to indicate for the i and j corresponding to the k^{th} value in [C8] that

$$i_k^2 + j_k^2 \geq k \qquad [C9]$$

In the first n values of i there are

$$T = \sum_{i=1}^{n} i \qquad [C10]$$

terms where T is

$$T = \frac{n(n+1)}{2} \qquad [C11]$$

The j = 1 term is the minimum value of $i^2 + j^2$ for any value of i. Since, for i = n

$$n^2 + j^2 > n^2 \qquad [C12]$$

if

$$n^2 \geq \frac{n(n+1)}{2} \qquad [C13]$$

inequality [C9] will be obtained. Since [C13] is valid for

$$n \geq 1 \qquad [C14]$$

then [C9] holds and the right side of [C7] may be written

$$\frac{a^8 a_{ij}^2}{[S\pi^4]^2} < \sum_{i=1}^{\infty} \sum_{j=1}^{i} \frac{1}{[i^2 + j^2]^4} \leq 2 \frac{a^8 a_{ij}^2}{S\pi^4} \sum_{i=1}^{\infty} \frac{1}{k^4} \qquad [C15]$$

The advantage of the last series is that its sum has a bound. The partial sum for the first $2^t - 1$ terms is

$$Q_{2t-1} = \frac{1}{1^4} + \frac{1}{2^4} + \frac{1}{3^4} + \cdots + \frac{1}{(2^t - 1)^4} \qquad [C16]$$

which is less term by term than

$$Q'_{2t-1} = \frac{1}{1^4} + \left(\frac{1}{2^4} + \frac{1}{2^4}\right) + \frac{1}{4^4} + \cdots + \frac{1}{4^4} + \left(\frac{1}{(2^{t-1})^4} + \cdots \frac{1}{(2^{t-1})^4}\right) \qquad [C17]$$

which is

$$Q'_{2t-1} = \frac{1}{1^4} + \frac{1}{2^3} + \left(\frac{1}{2^3}\right)^2 + \cdots + \left(\frac{1}{2^3}\right)^{t-1} \qquad [C18]$$

thus

$$Q'_{2t-1} = \frac{1 - \left(\frac{1}{2^3}\right)^t}{1 - \frac{1}{2^3}} = \frac{2^3}{2^3 - 1} - \frac{\left(\frac{1}{2^3}\right)^{t-1}}{2^3 - 1} \qquad [C19]$$

The second of the two terms is always negative and goes to zero as $2^t - 1$ increases. Thus the sum of the primed series from the $2^t - 1$ term to the end, Q , is less than the second term on the right side of [19]

$$Q'_R < \frac{\left(\frac{1}{2^3}\right)^{t-1}}{2^3 - 1} \qquad [C20]$$

Since the primed series is greater than by term than the k series, the sum of the k series over the same terms must also be bound by the same amount.

$$\sum_{k=2^t}^{\infty} \frac{1}{k^4} < \frac{\left(\frac{1}{2^3}\right)^{t-1}}{2^3 - 1} \qquad [C21]$$

The original series is smaller than the k series term by term, therefore, since

$$\int_o^a \int_o^b w^2(x,y,t)dx\,dy = \sum_{i=1}^{2^t-1} \frac{a^8 a_i^2}{[S\pi^4]^2} \frac{1}{[m_i^2 + n_i^2]^4} + \sum_{i=2^t}^{\infty} \frac{a^8 a_i^2}{[S\pi^4]^2 [n_i^2]} \qquad [C22]$$

then

$$\int_o^a \int_o^b w^2(x,y,t)dx\,dy \leq \sum_{i=1}^{2^t-1} \frac{a^8 a_i^2}{[S\pi^4]^2} \frac{1}{[m_i^2 + n_i^2]^4} + \frac{a^8}{[S\pi^4]^2} \frac{a_i^2\left(\frac{1}{2^3}\right)^{t-1}}{2^3 - 1} \qquad [C23]$$

and

$$\int_0^a \int_0^b \varpi\,(x,y,t)\,dx\,dy - \sum_{i=1}^{2^t-1} \frac{a^8 a_i^2}{[S\pi^4]^2 [m_i^2 + n_i]^4} \leq \frac{a^8}{[S\pi^4]^2} \frac{a_i^2 \frac{1}{2^3}^{t-1}}{2^3 - 1} \qquad [C24]$$

The inequality may be used either to place a bound on the error for a fixed number of modes considered in the evaluation, or conversely, it may be used to select the number of modes which must be considered to keep the error below a certain level. It should be noted that the value of a_i in [C24] is the result after control and must be chosen conservatively enough to reflect the induced error as well as that already present. Once the bound on the error has been selected t may be determined from [C24]. This equation was based on the use of $2^t - 1$ terms in the series, consequently a square $n \times n$ array of modes cannot be used for which

$$\frac{n(n+1)}{2} > 2^t - 1$$

Finally, the tightness of the bound is dependent on how closely the k series approximates the true series for the terms after the $2^t - 1$ term. The bound may be tightened by observing actual deviations and adjusting the inequality [C24] by the appropriate amount.

APPENDIX D

Mirror Displacement Feedback

The actuators considered in this appendix are modeled as types which are being considered for actual usage[6-8]. This model consists of a pure displacement actuator acting against a spring and a backing plate which is stiff relative to the spring. To obtain a specified force the displacement actuator is commanded to a new location relative to the undeformed mirror.

If the mirror has deformed, the displacement of the mirror will alter the magnitude of the applied force. It is assumed, arbitrarily, that one form of this displacement feedback might take is

$$p_i(x,y,t) = \alpha_i(t)\beta_i(x,y) - K w_i(x,y,t) \qquad [D1]$$

where $p_i(x,y,t)$ is the force density applied by the i^{th} actuator, and where

$$w_i(x,y,t) = w(x,y,t) \qquad [D2a]$$

over the i^{th} pad area, and

$$w_i(x,y,t) = 0 \qquad [D2b]$$

elsewhere, and

$$\alpha_i(t) = \frac{K l_i(t)}{\iint \beta_i(x,y)\,dx\,dy} \qquad [D3]$$

$w_i(x,y,t)$ may be expanded as

$$w_i(x,y,t) = \sum_{j=1}^{\infty} c'_{ij}(t)u_j(x,y) \qquad [D4]$$

where

$$c'_{ij}(t) = \int\int_{\Gamma} w_i(x,y,t)u_j(x,y)dx\ dy \qquad [D5]$$

Since $w_i(x,y,t)$ is zero except over the pad area of the i^{th} pad [D5] can be written

$$c'_{ij}(t) = \int_{\substack{i^{th}\ pad\\ area}} \int w(x,y,t)u_j(x,y)dx\ dy \qquad [D6]$$

Substituting the modal expansion of $w(x,y,t)$ yields

$$c'_{ij}(t) = \int_{\substack{i^{th}\ pad\\ area}} \int \sum_{k=1}^{\infty} c_k(t)u_k(x,y)u_j(x,y)dx\ dy \qquad [D7]$$

Interchanging the order of summation and integration yields

$$c'_{ij} = \sum_{k=1}^{\infty} c_k(t) \int_{\substack{i^{th}\ pad\\ area}} \int u_k(x,y)u_j(x,y)dx\ dy \qquad [D8]$$

The total feedback force, $f_s(x,y,t)$ is

$$f_s(x,y,t) = - K \sum_{i=1}^{N} w_i(x,y,t) \qquad [D9]$$

Substituting [D4] into [D9]

$$f_s(x,y,t) = - K \sum_{i=1}^{N} \sum_{j=1}^{\infty} c'_{ij}(t) u_j(x,y) \qquad [D10]$$

Interchanging the order of summation

$$f_s(x,y,t) = - K \sum_{j=1}^{\infty} u_j \sum_{i=1}^{N} c'_{ij}(t) \qquad [D11]$$

By comparison with equation [12b] $f_s(x,y,t)$ can be expressed modally as

$$f_s(x,y,t) = \sum_{j=1}^{\infty} a'_j(t) u_j(x,y) \qquad [D12]$$

where

$$a'_j(t) = - K \sum_{i=1}^{N} c'_{ij}(t) \qquad [D13]$$

Equations [D13] and [D8] can be used to put the expression for $a'_j(t)$ into a different form

$$- \frac{a'_j(t)}{K} = \sum_{i=1}^{N} \sum_{k=1}^{\infty} c_k(t) \int_{\substack{i^{th} \\ area}} \int_{pad} u_k(x,y) u_j(x,y) dx\, dy \qquad [D14]$$

Interchanging the order of summation

$$-\frac{a_j(t)}{K} = \sum_{k=1}^{\infty} c_k(t) \sum_{i=1}^{N} \int_{\substack{i\text{th} \\ \text{area}}} \int_{\text{pad}} u_k(x,y)u_j(x,y)dx\,dy \qquad [D15]$$

thus

$$-a'(t) = +KZ\,c(t) \qquad [D16]$$

where Z is an $\infty \times \infty$ matrix which has individual elements of

$$z_{jl} = \sum_{i=1}^{N} \int_{\substack{i\text{th} \\ \text{area}}} \int_{\text{pad}} u_j(x,y)u_l(x,y)dx \qquad [D17]$$

and where the spring constants are all assumed equal.

The matrix Z is located in a local feedback loop around the diagonal plant matrix since it describes amplitudes in the force modes as a function of the displacement mode amplitudes. Since, in general, the elements of Z are non-zero, this feedback causes the system to become coupled. In this particular application the coupling exists but can be made to have negligible amplitude. Since the displacement of the mirror is on the order of microinches the spring constant is adjusted so that the actuator throw required is on the order of inches.

Alternatively, a form of spring feedback may occur which can be treated without introducing coupling. Suppose that the expression for $p_i(x,y,t)$ is

$$p_i(x,y,t) = \frac{K(l_{d_i} - l_{m_i})\beta_i(x,y)}{\iint_\Gamma \beta_i(x,y)dx\ dy} \qquad [D18]$$

which would be obtained by decreasing the pad area until the mirror displacement over the pad area is constant. This, depending on the manner in which the pad is bonded to the mirror, appears to be a reasonable assumption. Expanding [D18] yields

$$p_i(x,y,t) = \frac{Kl_{d_i}\beta_i(x,y)}{\iint_\Gamma \beta_i(x,y)dx\ dy} - \frac{Kl_{m_i}\beta_i(x,y)}{\iint_\Gamma \beta_i(x,y)dx\ dy} \qquad [D19]$$

This equation can be analyzed by a procedure similar to the preceding paragraph, or equivalent results may be determined from an inspection of the appropriate block diagram. Proceeding as previously, the second term in [D19] is

$$f_{s_i}(x,y,t) = -Kl_{m_i}\beta_i(x,y)\Big/\iint_\Gamma \beta_i(x,y)dx\ dy \qquad [D20]$$

where l_m is the constant value of $w(x,y,t)$ over the pad area. It is desired to express $f_s(x,y,t)$ in a modal expansion

$$f_{s_i}(x,y,t) = \sum_{j=1}^{\infty} a'_{ij}(t)u_j(x,y) \qquad [D21]$$

where

$$a'_{ij}(t) = -\left(K\Big/\iint_\Gamma \beta_i(x,y)dx\ dy\right)\iint_\Gamma w_i(x,y,t)\beta_i(x,y)u_j(x,y)dx\ dy \qquad [D22]$$

Since $w_i(x,y,t)$ is constant over the pad area and $\beta_i(x,y)$ is zero elsewhere [D22] becomes

$$a'_{ij}(t) = \frac{-K l_{m_i}(t)}{\iint_\Gamma \beta_i(x,y)\,dx\,dy} \int_{\substack{i^{th}\\ \text{area}}} \int_{\text{pad}} \beta_i(x,y) u_j(x,y)\,dx\,dy \qquad [D23]$$

The integral has been previously evaluated as h_{ji} (Eq. [18b]), therefore

$$a'_{ij}(t) = \frac{-K l_{m_i}(t)}{\iint_\Gamma \beta_i(x,y)\,dx\,dy} h_{ji} \qquad [D24]$$

and if the integral of $\beta_i(x,y)$ is equal to that of $\beta_j(x,y)$ then

$$a'_j(t) = \frac{-K}{\iint_\Gamma \beta_i(x,y)\,dx\,dy} H l^N(t) \qquad [D25]$$

where

$$l^N(t) = \begin{bmatrix} w(x_j,y_j,t) \\ \vdots \\ w(x_j,y_N,t) \end{bmatrix} = w^N(t) \qquad [D26]$$

In this case the general result indicates that there is coupling in the system. If the system is assumed to have only finite eigenfunction content then

$$w^N = \sum_{i=1}^{N} c_i(t)u_i(x,y) \qquad [D27]$$

If [D27] is placed in matrix form

$$w^N = U^N c(t) \qquad [D28]$$

where

$$U^N = \begin{bmatrix} U_1(x_1,y_1) & \cdots & U_N(x_1,y_1) \\ \vdots & \ddots & \vdots \\ U_1(x_N,y_n) & \cdots & U_N(x_N,y_n) \end{bmatrix} \qquad [D29]$$

The spring feedback loop as described by [D18] and [D25] is shown in Figure D-1

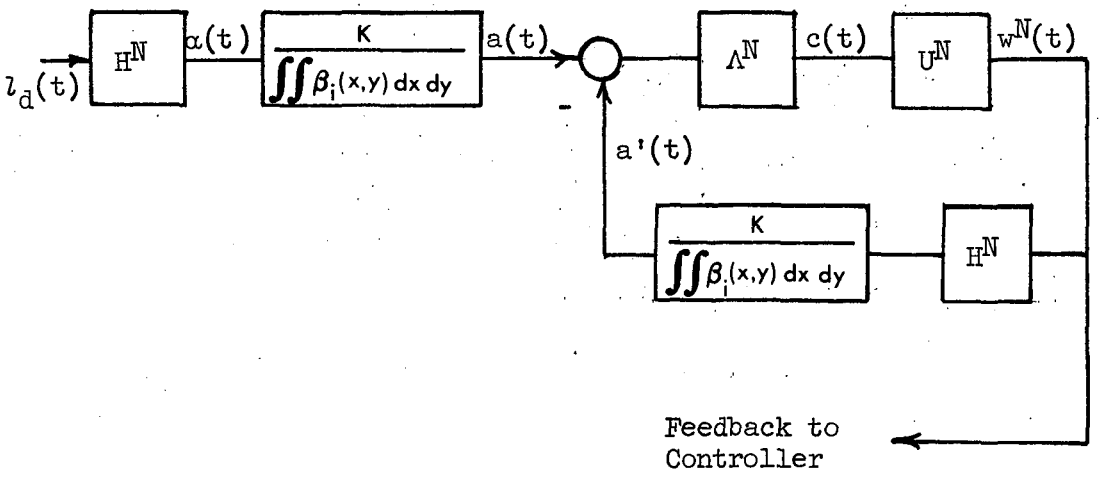

Figure D-1

The spring feedback loop.

As indicated previously, under appropriate conditions, the matrix can be written as the product of a diagonal matrix and a nondiagonal matrix as in 34 . In this case the spring feedback loop becomes that shown in Figure D-2

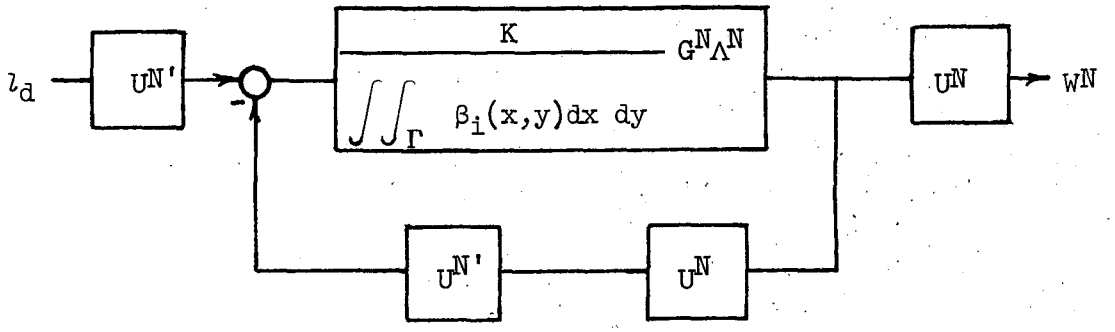

Figure D-2

The spring feedback loop for $H^N = G^N U^{N'}$.

Both G^N and $\dfrac{K}{\iint_\Gamma \beta_i(x,y)dx\,dy}$ are diagonal elements. Consequently, when $U^{N'} = U^{N-1}$ the system is decoupled (see Fig. D-3) and the effects of the spring feedback can be readily included in the system design.

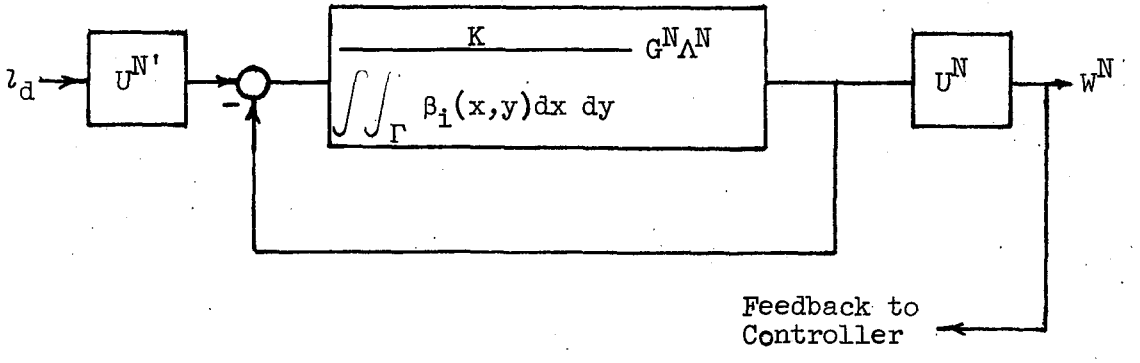

Figure D-3

The decoupled spring feedback loop.

In summary, under a specific set of assumptions, the effects of the mirror displacement feedback can be treated without introducing coupling effects into the system. In general, coupling effects are present, however, the mirror displacement feedback is rendered negligible through an appropriate choice of spring constant.

BIBLIOGRAPHY

1. Born, M., and Wolf, E., Principles of Optics, Second Edition, MacMillan Company, New York, N.Y., 1964.

2. Courant, R., and Hilbert, D., Methods of Mathematical Physics, First English Edition, Interscience Publishers, Inc., New York, N.Y., 1937.

3. Creedon, J. F., and Robertson, H. J., "Evaluation of Multipoint Interaction in the Design of a Thin Diffraction-Limited Active Mirror," IEEE Trans. on Aerospace and Electronics Systems, Vol. AES-5, No. 2, March 1969, pp. 287-293.

4. Frederick, L. W., ed., "Applications in Astronomy Suitable for Study by Means of Manned Orbiting Observatories and Related Instrumentation and Operational Requirements," NASA CR-52897 (Vol. 1) and NASA CR-52902 (Vol. 2) Leander McCormick Observatory, University of Virginia, Charlottesville, Va., 1963.

5. Goody, R. M., Atmospheric Radiation-I Theoretical Basis, Oxford Monographs on Meteorology, Oxford University Press, Amen House, London, England, 1964.

6. Gould, L. A., and Murray-Lasso, M. A., "On the Modal Control of Distributed Systems With Distributed Feedback," IEEE Trans. on Automatic Control, Vol. AC-11, No. 4, October 1966, pp. 729-736.

7. Greensite, A. L., "Analyses and Design of Space Vehicle Flight Control Systems," Vol. XII - Attitude Control in Space. NASA CR-831, General Dynamics Corp., San Diego, Calif., August 1967.

8. Howell, W. E., "Technology for a Manned Orbiting Telescope," Proc. of the Space Optical Technology Conference, Vol. 1, NASA-Langley Research Center, Langley Station, Hampton, Va., April 1966.

9. Lindgren, A. G., "A Note on Stability and Design of Interacting Multivariable Control Systems," IEEE Trans. on Automatic Control, Vol. AC-11, No. 2, April 1966, pp. 314-315.

10. Robertson, H. J., et al., "Active Optical System for Spaceborne Telescopes," NASA CR-66297, Perkin-Elmer Co., Norwalk, Connecticut, October 14, 1966.

11. Robertson, H. J., et al., "Active Optical System for Spaceborne Telescopes," Vol. II, NASA CR-66489, Perkin-Elmer Co., Norwalk, Connecticut, December 7, 1967.

12. Robertson, H. J., "Development of an Active Optics Concept Using a Thin Deformable Mirror," NASA CR-1593, Perkin-Elmer Co., Norwalk, Connecticut, 1970.

13. Timoshenko, S., and Woinowsky-Kreiger, S., Theory of Plates and Shells, Second Edition, McGraw-Hill Book Company, New York, N.Y., 1959.

14. Truxal, J. G., "Control Systems - Some Unusual Design Problems," Chapter 4, Adaptive Control Systems, Mishken, E., and Braun, L., (eds.), McGraw-Hill Book Company, Inc., New York, N.Y., 1961.

15. Wylie, C. R., Jr., Advanced Engineering Mathematics, Third Edition, McGraw-Hill Book Company, New York, N.Y., 1966.